1

Linear Response Theory Applications to IR Spectra of H-Bonded Cyclic Dimers Taking into Account the Surrounding. Updating Contributions Involving Davydov Coupling, Fermi Resonances and Electrical Anharmonicity

Paul Blaise and Olivier Henri-Rousseau

Laboratory of Mathematics and Physics, 52 Av. Paul Alduy, 66100 Perpignan, France

1.1 Introduction

This chapter is devoted to the application of the Henri-Rousseau and Blaise model [1] which has incorporated quantum mechanically the damping of the H-bond bridge into the Maréchal and Witkowski model [2] to the experimental infrared (IR) lineshapes of cyclic centrosymmetric dimers. In Figure 1.1, are depicted for example linear and cyclic H-bonded carboxylic acids.

One may distinguish the length q of O—H bond and Q one of the H-bond. In Figure 1.2 are recapitulated the connections between the present applied theory and diverse older ones.

1.2 Dimer Strong Anharmonic Coupling Theory

1.2.1 Different Theoretical Situations

1.2.1.1 Strong Anharmonic Coupling Within Adiabatic Approximation For Monomer

Let us consider a single H-bonded system where X and Y are nucleophilic substituents such as oxygen or nitrogen (See **Figure 1.3**). Define $\mathbf{q}$ and $\mathbf{Q}$ as the operators corresponding to the lengths of X–H and X–Y bonds. Besides, both these lengths are oscillating, the first one at high frequency and the last one H-bond bridge at low frequency.

Now suppose that a strong anharmonic coupling may occur between the X-H high-frequency mode $\mathbf{q}$ and the X$\cdots$Y low-frequency mode $\mathbf{Q}$.

Within the strong anharmonic coupling theory, it is assumed a linear dependence of the high-frequency mode $\omega(\mathbf{Q})$ on the H-bond bridge coordinate $\mathbf{Q}$, according to:

$$\omega(\mathbf{Q}) = \omega^\circ + b\mathbf{Q} \quad \text{with} \quad b < 0 \tag{1.1}$$

where ω° is the angular frequency of a isolated X–H bond and b some parameter.

Spectroscopy and Computation of Hydrogen-Bonded Systems, First Edition.
Edited by Marek J. Wójcik and Yukihiro Ozaki.

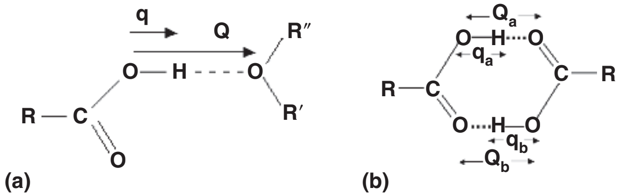

Figure 1.1 (a) H-bond monomer and the coordinates. (b) H-bond dimer and the coordinates.

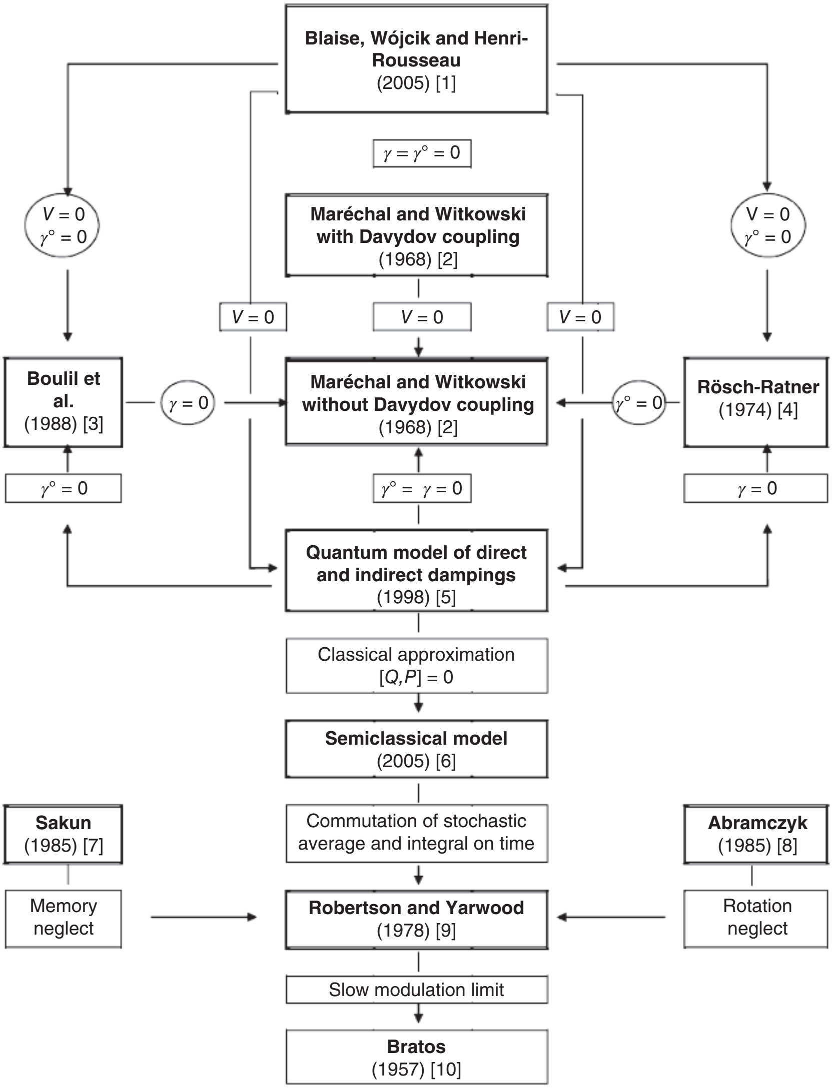

[1] P. Blaise, M.J. Wójcik and Olivier Henri-Rousseau J. Chem. Phys. 122, (2005) 064360 ; [2] Y. Maréchal and A. Witkowski, J. Chem. Phys. 48 (1968) 3677 ; [3] B. Boulil, O. Henri-Rousseau, P. Blaise, Chem. Phys. 126 (1988) 263 ; [4] N. Rösch, M. Ratner, J. Chem. Phys. 61 (1974) 3344. ; [5] O. Henri-Rousseau, P. Blaise, Adv. Chem. Phys. Vol 103 in I. Prigogine, S.A. Rice, (Eds) John Wiley&Sons, New York, 1998 p.1-186 ; [6] P. Blaise, P-M. Déjardin and O. Henri-Rousseau, Chem. Phys, 313 (2005) 177. ; [7] V. Sakun, Chem. Phys. 99 (1985) 457. ; [8] H. Abramczyk, Chem. Phys.,94 (1985) 91. ; [9] G. Robertson, J. Yarwood, Chem. Phys. 32 (1978) 267. ; [10] S. Bratos and D. Hadzi, J. Chem. Phys. 27 (1957) 991. 40

Figure 1.2 Connections between the present theory and different older models.

The full Hamiltonian may be partitioned as follows:

$$\mathbf{H}_{\text{tot}} = \mathbf{H}_{\text{fast}} + \mathbf{H}_{\text{slow}} \tag{1.2}$$

The Hamiltonian of the slow mode may be viewed as either harmonic or anharmonic (Morse-like)

$$\text{Harmonic: } \mathbf{H}_{\text{slow}} = \frac{\mathbf{P}^2}{2M} + \frac{1}{2}M\Omega^2\mathbf{Q}^2$$

$$\text{Morse like: } \mathbf{H}_{\text{slow}} = \frac{\mathbf{P}_i^2}{2M}\hbar\Omega + D_{\text{e}}\left[1 - \mathrm{e}^{-\beta_{\text{e}}\mathbf{Q}_i\sqrt{\frac{M\Omega}{\hbar}}}\right]^2$$

$$\text{with } \beta_{\text{e}} = \Omega\sqrt{\frac{M}{2D_{\text{e}}}}\sqrt{\frac{\hbar}{M\Omega}}$$

Here, **P** is the momentum coordinate of the slow mode of reduced mass M and angular frequency Ω, whereas D_{e} is the dissociation energy of the Morse curve.

The Hamiltonian $\mathbf{H}_{\text{fast}}$ is corresponding to the ν_{s}(X–H) high-frequency mode. Within the harmonic approximation and strong anharmonic coupling theory, it is:

$$\mathbf{H}_{\text{fast}} = \frac{\mathbf{p}^2}{2m} + \frac{1}{2}m(\omega(\mathbf{Q}))^2\mathbf{q}^2 = \frac{\mathbf{p}^2}{2m} + \frac{1}{2}M\omega^{\circ 2}\mathbf{q}^2 + m\omega^{\circ}b\mathbf{q}^2\mathbf{Q} + \frac{1}{2}mb^2\mathbf{q}^2\mathbf{Q}^2 \tag{1.3}$$

whereas **p** is the momentum coordinates for the fast mode.

The eigenvalue equations of the fast and slow harmonic modes are given respectively, neglecting the zero-point energy of the fast mode by:

$$\left(\frac{\mathbf{p}^2}{2m} + \frac{1}{2}M\omega^{\circ 2}\mathbf{q}^2\right)|\{k\}\rangle \equiv \mathbf{H}_{\text{free}}\,|\{k\}\rangle = \hbar\omega^{\circ}k\,|\{k\}\rangle$$

$$\left(\frac{\mathbf{P}^2}{2M} + \frac{1}{2}M\Omega^2\mathbf{Q}^2\right)|(n)\rangle = \hbar\Omega\left(n + \frac{1}{2}\right)|(n)\rangle \tag{1.4}$$

Within the adiabatic approximation the full Hamiltonian becomes simply:

$$\left[\mathbf{H}_{\text{adiab}}\right] = \sum_k \left[\mathbf{H}_I^{\{k\}}\right]|\{k\}\rangle\langle\{k\}|$$

where

$$\left[\mathbf{H}_I^{\{0\}}\right] = \frac{\mathbf{P}^2}{2M} + \frac{1}{2}M\Omega^2\mathbf{Q}^2; \quad \left[\mathbf{H}_I^{\{1\}}\right] = \frac{\mathbf{P}^2}{2M} + \frac{1}{2}M\Omega^2\mathbf{Q}^2 + \hbar b\mathbf{Q} + \hbar\omega^{\circ} \tag{1.5}$$

Figure 1.4 represents the absorption mechanism generating a coherent state.

It is possible to generalize the above approach by introducing together with the coupling of the fast mode to the H-bond bridge, another coupling of the fast mode with some bending mode according to:

$$\mathbf{H}_{\text{tot}} = \mathbf{H}_{\text{fast}} + \mathbf{H}^{\circ}{}_{\text{slow}} + \mathbf{H}^{\circ}{}_{\text{bend}}$$

with, by taking the H-bond bridge potential as Morse-like (See **Table 1.1**).

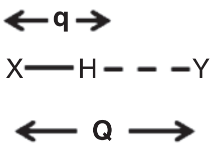

Figure 1.3 Coordinates of single H-bonded system.

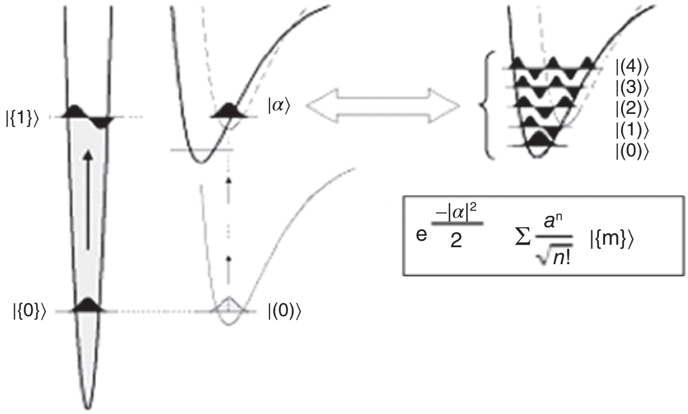

Figure 1.4 Physics of the absorption mechanism. The ground state of the slow mode H-bond bridge (corresponding to the ground state situation of the fast mode) becomes a coherent state $\alpha = \mathbf{a} \mid \alpha\rangle$ after excitation towards the first excited state of the fast mode.

Table 1.1 Different sorts of Hamiltonians.

$$\mathbf{H}_{\text{fast}} = \frac{\mathbf{p}^2}{2m} + \frac{1}{2} m \left(\omega^\circ + \alpha^\circ \mathbf{Q} + \beta \mathbf{Q}_\delta\right)^2 \mathbf{q}^2$$

$$\mathbf{H}^\circ_{\text{slow}} = \frac{\mathbf{P}^2}{2M} + D_{\text{e}} \left[1 - \mathrm{e}^{-\Omega \sqrt{\frac{M}{2D_{\text{e}}}} \mathbf{Q}}\right]^2$$

$$\mathbf{H}^\circ_{\text{bend}} = \frac{\mathbf{P}^2}{2M_\delta} + \frac{1}{2} M_\delta \Omega_\delta^2 \mathbf{Q}_\delta^2$$

where $\mathbf{Q}_\delta$ and $\mathbf{P}_\delta$ are respectively the position and momentum coordinates of the bending mode having Ω_δ as angular frequency and M_δ as reduced mass.

1.2.1.2 Introduction of Fermi Resonances

Now, there is the possibility to introduce Fermi resonance [11] in this physical model as it is illustrated in Figure 1.5.

There is a coupling characterized by the parameter f_1^δ between the two situations evoked in Figure 1.5.

In the absence of damping, the full Hamiltonian involving Fermi resonances is:

$$\left[\mathbf{H}_{\text{Fermi}}\right] = \left[\mathbf{H}_{\text{Free}} + \mathbf{H}_{\text{slow}} + \mathbf{H}_{\text{Int}}\right] + \mathbf{H}_{\text{Bend}} + \mathbf{V}_{\text{Bend}} \tag{1.6}$$

Here, the three first right-hand side Hamiltonians are the components of the bare H-bond Hamiltonians without Fermi resonance given respectively by equations given in Table 1.1. Besides, the Hamiltonian $\mathbf{H}_{\text{Bend}}$ corresponding to the bending mode and the interaction $\mathbf{V}_{\text{Bend}}$ between the fast and bending modes are respectively:

$$\mathbf{H}_{\text{Bend}} = \frac{\mathbf{p}_\delta^2}{2m^\delta} + \frac{1}{2} m^\delta \left(\omega^\delta\right)^2 \mathbf{q}_\delta^2; \ \mathbf{V}_{\text{Bend}} = l^\delta \ \mathbf{q}\mathbf{q}_\delta^2 \tag{1.7}$$

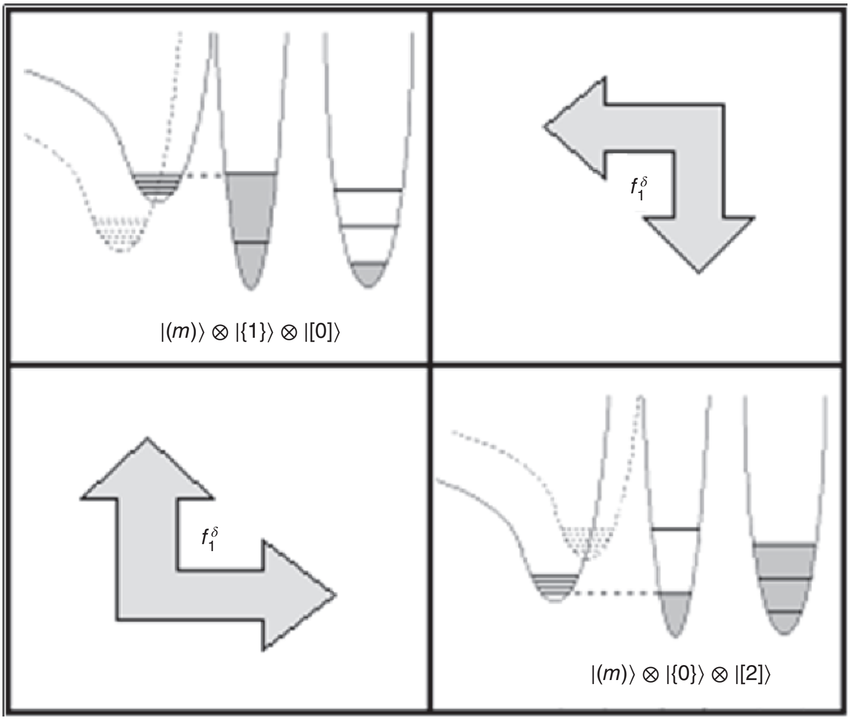

Figure 1.5 Fermi resonances interaction coupling parameters f_1^δ between two situations of the fast, slow, and bending modes. Source: Henri-Rousseau and Blaise 2008 [18]/John Wiley & Sons.

where $\mathbf{q}_\delta$ and $\mathbf{p}_\delta$ are respectively the position and momentum coordinates of the bending mode of reduced mass m^δ and ω^δ its angular frequency, whereas l^δ is the coupling parameter between the fast and bending modes. The eigenvalue equations of the harmonic Hamiltonians corresponding respectively to the fast and slow modes are respectively given by equations given by Eqs. (1.4) whereas that dealing with the bending modes is, ignoring the zero-point energy:

$$\mathbf{H}_{\text{Bend}} \left|[l^\delta]\right\rangle = l^\delta \hbar\omega^\delta \left|[l^\delta]\right\rangle \tag{1.8}$$

Now, within the adiabatic approximation. The Hamiltonian (1.6) becomes:

$$\left[\mathbf{H}^{\text{Adiab}}_{\text{Fermi}}\right] = \left[\mathbf{H}_{\text{Adiab}}\right] + \left[\mathbf{V}_{\text{Bend}}\right] + \left[\mathbf{H}_{\text{Bend}}\right] \tag{1.9}$$

The different Hamiltonians are given as follows:

$$\left[\mathbf{H}_{\text{Adiab}}\right] = \left[\mathbf{H}_I^{\{1\}}\right] |\{1\}\rangle\langle\{1\}| + \left[\mathbf{H}_I^{\{0\}}\right] |\{0\}\rangle\langle\{0\}|$$

$$\left[\mathbf{H}_I^{\{k\}}\right] = \frac{\mathbf{P}^2}{2M} + \frac{1}{2}M\Omega^2\mathbf{Q}^2 + kb\mathbf{Q} + k\hbar\omega^\circ$$

$$\left[\mathbf{H}_{\text{Bend}}\right] = 2\hbar\omega^\delta\, |[2]\rangle\langle[2]|$$

$$\left[\mathbf{V}_{\text{Bend}}\right] = \left[|\{0\}\rangle|[2]\rangle\langle[0]|\langle\{1\}|\right] \hbar f^{\,\delta} + hc$$

Here, f_1^δ is the anharmonic coupling parameter involved in the Fermi resonance which is a function of l^δ.

As a consequence of the above equations, the full Hamiltonian describing the fast mode coupled to the H-bond bridge (via the strong anharmonic coupling theory) and the bending mode (via the Fermi resonance process) may be written within the tensorial basis (1.10) according to [12]:

$$\begin{pmatrix} \left|\Psi_a\left(\{0\}\,(m)\,[0]\right)\right\rangle \\ \left|\Psi_b\left(\{1\}\,(m)\,[0]\right)\right\rangle \\ \left|\Psi_c\left(\{0\}\,(m)\,[2]\right)\right\rangle \end{pmatrix} = \begin{pmatrix} |\{0\}\,(m)\,[0]\rangle \\ |\{1\}\,(m)\,[0]\rangle \\ |\{0\}\,(m)\,[2]\rangle \end{pmatrix} \tag{1.10}$$

$$\left[\mathbf{H}^{\mathrm{Adiab}}_{\mathrm{Fermi}}\right] = \begin{pmatrix} \mathbf{H}^{\{0\}}_{II} & 0 & 0 \\ 0 & \mathbf{H}^{\{1\}}_{II} & \hbar f^{\,\delta}_{\,1} \\ 0 & \hbar f^{\,\delta}_{\,1} & \mathbf{H}^{\{0\}}_{II} + 2\hbar\omega^\delta_1 \end{pmatrix} \tag{1.11}$$

1.2.1.3 H-Bonded Centrosymmetric Dimer

Now, look at an H-bonded dimer. It will take place in a Davydov coupling [13]. Within the anharmonic coupling, the physics of the system may be viewed in Figure 1.6.

It may be observed that because of the symmetry of the dimer, there is a $\mathbf{C}_2$ operator (with $\mathbf{C}_2^2 = \hat{\mathbf{1}}$), which exchanges the coordinates $\mathbf{Q}_i$ of the two slow modes H-bond bridges of the cyclic dimer according to:

$$\mathbf{C}_2\mathbf{Q}_a = \mathbf{Q}_b;\quad \mathbf{C}_2\mathbf{Q}_b = \mathbf{Q}_a;\quad \mathbf{C}_2\mathbf{P}_a = \mathbf{P}_b;\quad \mathbf{C}_2\mathbf{P}_b = \mathbf{P}_a \tag{1.12}$$

Ignoring for the present time the interaction between the two moieties and assuming that, within each moiety, the adiabatic approximation may be performed as for a

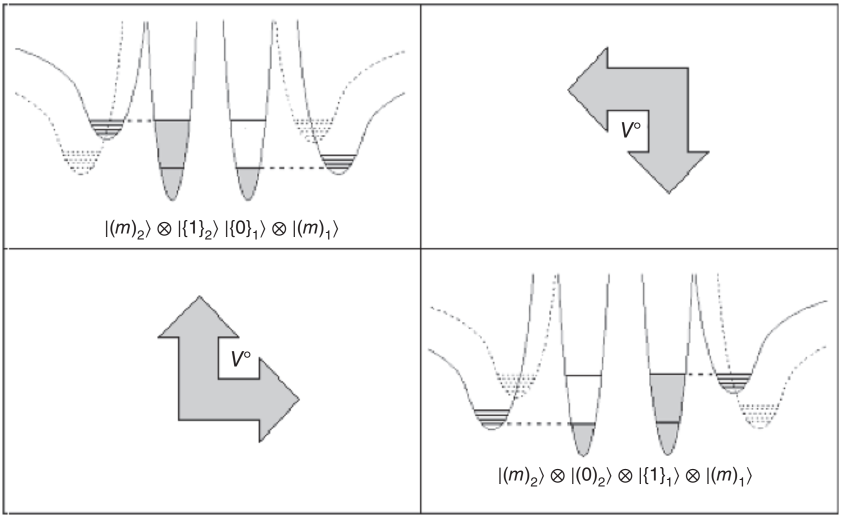

Figure 1.6 Davydov coupling interactions. Source: Henri-Rousseau and Blaise 2008 [18]/John Wiley & Sons.

single H-bond, the Hamiltonian of the symmetric dimer embedded in the thermal bath, is:

$$\left[\mathbf{H}^{\{\text{Adiab}\}}\right] = \left[\mathbf{H}^{\{\text{Adiab}\}}\right]_a + \left[\mathbf{H}^{\{\text{Adiab}\}}\right]_b \tag{1.13}$$

In Eq. (1.13), the two first right-hand side terms are the adiabatic Hamiltonians of each moiety. They are given by an expression of the same form which is:

$$\left[\mathbf{H}^{\{\text{Adiab}\}}\right]_i = \left[\mathbf{H}_{II}^{\{0\}}\right]_i \left|\{0\}_i\right\rangle\left\langle\{0\}_i\right| + \left[\mathbf{H}_{II}^{\{1\}}\right]_i \left|\{1\}_i\right\rangle\left\langle\{1\}_i\right| \quad \text{with } i = a, b$$

$\left|\{k\}_i\right\rangle$ are the eigenkets of the Hamiltonians of the fast modes harmonic oscillators, whereas the Hamiltonians of each moiety are respectively:

$$\begin{aligned}\left[\mathbf{H}^{\circ\{0\}}_{II}\right]_i &= \left[\mathbf{H}^{\{\text{Slow}\}}\right]_i \\ \left[\mathbf{H}^{\circ\{1\}}_{II}\right]_i &= \left[\mathbf{H}^{\{\text{Slow}\}}\right]_i + b\mathbf{Q}_i + \hbar\omega^\circ + \left[\mathbb{H}^{\{\text{Int}\}}_{II}\right]_i\end{aligned}$$

Here, the last term is the interacting coupling with the thermal bath that we shall ignore in the present simplified exposition. The Hamiltonian of the cyclic dimer involving Davydov coupling between the first excited state of the high-frequency oscillator *a* of one moiety and the excited state of the oscillator *b* of the other moiety and *vice versa* is,

$$\left[\mathbb{H}_{\text{Dav}}\right] = \left[\mathbf{H}^{\{\text{Adiab}\}}\right]_a + \left[\mathbf{H}^{\{\text{Adiab}\}}\right]_b + \mathbf{V}_{\text{Dav}} \tag{1.14}$$

The Davydov coupling Hamiltonian $\mathbf{V}_{\text{Dav}}$ appearing in this equation may be written either simply or as a function of the two slow modes coordinates [14]:

$$\begin{aligned}\mathbf{V}_{\text{Dav}} &= \mathbf{V}^\circ \left[\left|\{1\}_a\right\rangle\left\langle\{0\}_b\right| + \left|\{0\}_a\right\rangle\left\langle\{1\}_b\right|\right] \\ \mathbf{V}_{\text{Dav}}\left(Q_1, Q_2\right) &= \mathbf{V}_{\text{Dav}} + \Theta\left(Q_1 + Q_2\right)\left[\left|\{1\}_a\right\rangle\left\langle\{0\}_b\right| + \left|\{0\}_a\right\rangle\left\langle\{1\}_b\right|\right]\end{aligned}$$

where Θ is a dimensionless parameter governing the linear dependence of the Davydov coupling operator on the H-bond bridge coordinates.

When ignoring the Θ coupling, then, within the following basis:

$$\begin{pmatrix} \left|\mathbf{\Phi}^{\{0,0\}}_{\{a,b\}}\right\rangle \\ \left|\mathbf{\Phi}^{\{1,0\}}_{\{a,b\}}\right\rangle \\ \left|\mathbf{\Phi}^{\{0,1\}}_{\{a,b\}}\right\rangle \end{pmatrix} = \begin{pmatrix} \left|\{0\}_a\right\rangle \otimes \left|\{0\}_b\right\rangle \\ \left|\{1\}_a\right\rangle \otimes \left|\{0\}_b\right\rangle \\ \left|\{0\}_a\right\rangle \otimes \left|\{1\}_b\right\rangle \end{pmatrix} \tag{1.15}$$

the Davydov Hamiltonian (1.14) takes the matrix form:

$$\left[\mathbb{H}_{Dav}\right] = \begin{pmatrix} \left[\mathbf{H}^{\{0,0\}}_{II}\right] & 0 & 0 \\ 0 & \left[\mathbf{H}^{\{1,0\}}_{II}\right] & \mathbf{V}_{Dav} \\ 0 & \mathbf{V}_{Dav} & \left[\mathbf{H}^{\{0,1\}}_{II}\right] \end{pmatrix} \tag{1.16}$$

with respectively:

$$\left[\mathbf{H}_{II}^{\{0,0\}}\right] = \sum_i \left(\frac{\mathbf{P}_i^2}{2M} + \frac{M\Omega^2 \mathbf{Q}_i^2}{2} \right) \quad \text{with} \quad i = a, b$$

$$\left[\mathbf{H}_{II}^{\{1,0\}}\right] = \sum_i \left(\frac{\mathbf{P}_i^2}{2M} + \frac{M\Omega^2 \mathbf{Q}_i^2}{2} + b\mathbf{Q}_i \right) + \hbar\omega^\circ$$

Then, owing to the symmetry properties given by Eqs. (1.12), it appears that the parity operator exchanges the two last Hamiltonians:

$$\mathbf{C}_2 \left[\mathbf{H}_{II}^{\{1,0\}}\right] = \left[\mathbf{H}_{II}^{\{0,1\}}\right] \tag{1.17}$$

To diagonalize the Davydov Hamiltonian, one may perform the following basis change.

$$\begin{pmatrix} \left| \boldsymbol{\Phi}_{\{a,b\}}^{\{0,0\}} \right\rangle \\ \left| \boldsymbol{\beta}_{\{1,0\}\leftrightarrow\{0,1\}}^{(+)} \right\rangle \\ \left| \boldsymbol{\beta}_{\{1,0\}\leftrightarrow\{0,1\}}^{(-)} \right\rangle \end{pmatrix} = \begin{pmatrix} \left| \boldsymbol{\Phi}_{\{a,b\}}^{\{0,0\}} \right\rangle \\ \left| \boldsymbol{\Phi}_{\{a,b\}}^{\{1,0\}} \right\rangle + \hat{\mathbf{C}}_2 \left| \boldsymbol{\Phi}_{\{a,b\}}^{\{0,1\}} \right\rangle \\ \left| \boldsymbol{\Phi}_{\{a,b\}}^{\{1,0\}} \right\rangle - \hat{\mathbf{C}}_2 \left| \boldsymbol{\Phi}_{\{a,b\}}^{\{0,1\}} \right\rangle \end{pmatrix} \tag{1.18}$$

Then the Davydov Hamiltonian becomes:

$$\mathbb{H}_{\text{Dav}} = \begin{pmatrix} \left[\mathbf{H}_{II}^{\{0,0\}}\right] & 0 & 0 \\ 0 & \left[\mathbf{H}_{II}^{\{1,0\}} + \mathbf{V}^\circ \hat{\mathbf{C}}_2\right] & 0 \\ 0 & 0 & \left[\mathbf{H}_{II}^{\{1,0\}} - \mathbf{V}^\circ \hat{\mathbf{C}}_2\right] \end{pmatrix} \tag{1.19}$$

Moreover, to make tractable the action of the $\mathbf{C}_2$ operator, it is suitable to pass to the symmetrized coordinates and their conjugate momenta according to Figure 1.7.

In Table 1.2, are given the symmetrized coordinates in the Davydov coupling model.

Recall here, the improvement brought by Rekik et al. [15–17], by introducing the electrical anharmonicity. As quoted above, the dependence of the Davydov coupling on the slow mode coordinates reduces to one on $\boldsymbol{Q}_g$ through:

$$\boldsymbol{V}_{\text{D}}\left(Q_g\right) = V^\circ + \sqrt{2}\Theta \boldsymbol{Q}_g$$

Now, the action of the parity operator on the symmetrized operators and the symmetrized ground state and first excited state of Hamiltonian $\left[\mathbf{H}^{(\text{Slow})}\right]_i$ appearing in Table 1.2, is depicted in Figure 1.7:

Table 1.2 Symmetrized coordinates.

$\mathbf{Q}_g = \frac{1}{\sqrt{2}}\left[\mathbf{Q}_a + \mathbf{Q}_b\right]$	$\mathbf{Q}_u = \frac{1}{\sqrt{2}}\left[\mathbf{Q}_a - \mathbf{Q}_b\right]$	$\mathbf{P}_g = \frac{1}{\sqrt{2}}\left[\mathbf{P}_a + \mathbf{P}_b\right]$	$\mathbf{P}_u = \frac{1}{\sqrt{2}}\left[\mathbf{P}_a - \mathbf{P}_b\right]$
$\mathbf{C}_2\mathbf{Q}_g = \mathbf{Q}_g$	$\mathbf{C}_2\mathbf{Q}_u = -\mathbf{Q}_u$	$\mathbf{C}_2\mathbf{P}_g = \mathbf{P}_g$	$\mathbf{C}_2\mathbf{P}_u = -\mathbf{P}_u$

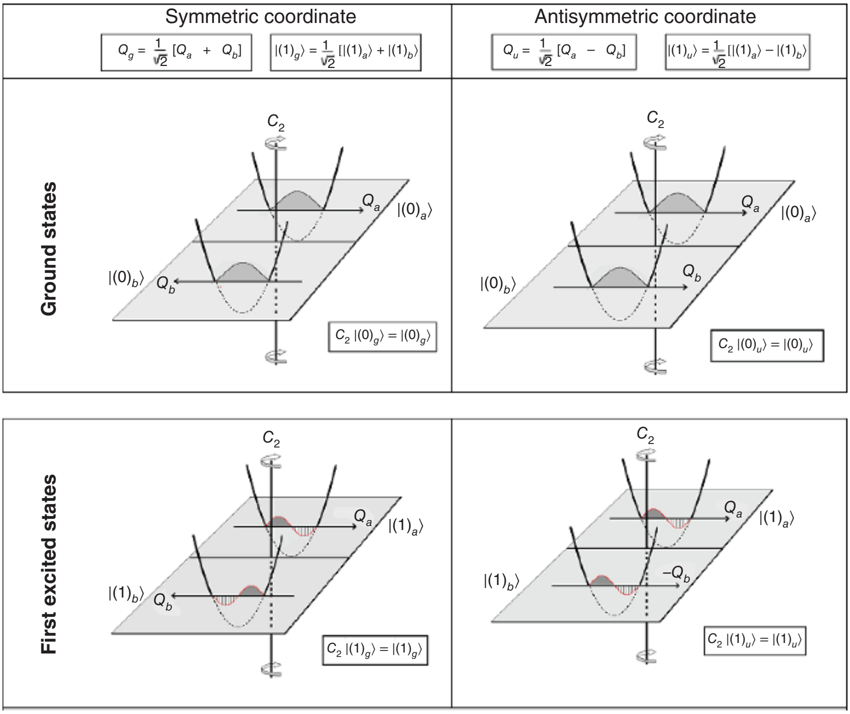

Figure 1.7 Action of the C_2 operator on coordinates and eigenstates. Source: Henri-Rousseau and Blaise 2008 [18] / John Wiley & Sons.

Next, we may consider the *kets* (1.18) as the result of the tensorial product of states, according to:

$$\begin{pmatrix} \left|\Phi^{\{0,0\}}_{\{g,u\}}\right\rangle \\ \left|\beta^{(+)}_{\{1,0\}\leftrightarrow\{0,1\}}\right\rangle \\ \left|\beta^{(-)}_{\{1,0\}\leftrightarrow\{0,1\}}\right\rangle \end{pmatrix} = \begin{pmatrix} \left|\{0\}_g\right\rangle \otimes \left|\,\{0\}_u\right\rangle \\ \left|\{1\}_g\right\rangle \otimes \left|\left\{\beta^{(+)}\right\}^{\{1\}}_{u^+}\right\rangle \\ \left|\{1\}_g\right\rangle \otimes \left|\left\{\beta^{(-)}\right\}^{\{1\}}_{u^-}\right\rangle \end{pmatrix} \tag{1.20}$$

with:

$$\begin{pmatrix} \left|\,\{0\}_g\right\rangle \\ \left|\,\{0\}_u\right\rangle \end{pmatrix} = \begin{pmatrix} \frac{1}{\sqrt{2}}\left[\left|\,\{0\}_a\right\rangle + \left|\,\{0\}_b\right\rangle\right] \\ \frac{1}{\sqrt{2}}\left[\left|\,\{0\}_a\right\rangle - \left|\,\{0\}_b\right\rangle\right] \end{pmatrix} \tag{1.21}$$

within the framework of the symmetrized coordinates the Hamiltonian (1.19) takes the form:

$$\left[\mathbb{H}_{\text{Dav}}\right] = \begin{pmatrix} \left[\mathbf{H}^{\{0\}}_{II}\right]_g & 0 & 0 & 0 & 0 \\ 0 & \left[\mathbf{H}^{\{1\}}_{II}\right]_g & 0 & 0 & 0 \\ 0 & 0 & \left[\mathbf{H}^{\{0\}}_{II}\right]_u & 0 & 0 \\ 0 & 0 & 0 & \left[\mathbf{H}^{\{1\}}_{(+)}\right]_{u^+} & 0 \\ 0 & 0 & 0 & 0 & \left[\mathbf{H}^{\{1\}}_{(-)}\right]_{u^-} \end{pmatrix} \quad \text{within} \quad \begin{pmatrix} \left|\{0\}_g\right\rangle \\ \left|\{1\}_g\right\rangle \\ \left|\{0\}_u\right\rangle \\ \left|\left\{\beta^{(+)}\right\}^{\{1\}}_{u^+}\right\rangle \\ \left|\left\{\beta^{(-)}\right\}^{\{1\}}_{u^-}\right\rangle \end{pmatrix} \tag{1.22}$$

with respectively:

$$\left[\mathbf{H}^{\{0\}}_{II}\right]_g = \frac{\mathbf{P}_g^2}{2M} + \frac{M\Omega^2\mathbf{Q}_g^2}{2}$$

$$\left[\mathbf{H}^{\{1\}}_{II}\right]_g = \frac{\mathbf{P}_g^2}{2M} + \frac{M\Omega^2\mathbf{Q}_g^2}{2} + \frac{1}{\sqrt{2}}\, b\mathbf{Q}_g + \hbar\omega^\circ$$

$$\left[\mathbf{H}^{\{0\}}_{II}\right]_u = \frac{\mathbf{P}_u^2}{2M} + \frac{M\Omega^2\mathbf{Q}_u^2}{2}$$

$$\text{and} \quad \left[\mathbf{H}^{\{1\}}_{(\pm)}\right]_u = \frac{\mathbf{P}_u^2}{2M} + \frac{M\Omega^2\mathbf{Q}_u^2}{2} + \frac{1}{\sqrt{2}} b\ \mathbf{Q}_u \pm \mathbf{V}^\circ\left(\hat{\mathbf{C}}_2\right)_u$$

1.2.1.4 Dimer Involving Damping, Davydov Coupling, and Fermi Resonances

Now, it is possible to introduce Fermi resonances in the precedent model taking into account direct and indirect dampings, together with the relaxation of the bending modes [18, 19].

For the special case of a single Fermi resonance, the physics related to this Hamiltonian is depicted in Figure 1.8.

Here, the right-hand side Hamiltonian is that dealing with the Fermi resonances occurring between the g excited state of the fast mode and the g first harmonics of the bending mode. For one Fermi resonance, this Hamiltonian is:

$$\left[\mathbb{H}^{\{1\}}_{\text{Fermi}}\right]_g = \begin{pmatrix} \left[\mathbb{H}^{\{1\}}_{II}\right]_g & \hbar f^{\ \delta} \\ \hbar f^{\ \delta} & [\mathbf{H}^{\{0\}}_{II}]_g + E \end{pmatrix}$$

Besides, the f_i is the coupling parameters involved in the Fermi resonances expressed as angular frequencies, whereas the Δ are the angular frequency gap:

$$E = \hbar\omega^\circ - \alpha^{\circ 2}\hbar\Omega + \hbar\Delta^\delta - \left(\omega^\circ - 2\omega_i^\delta\right)$$

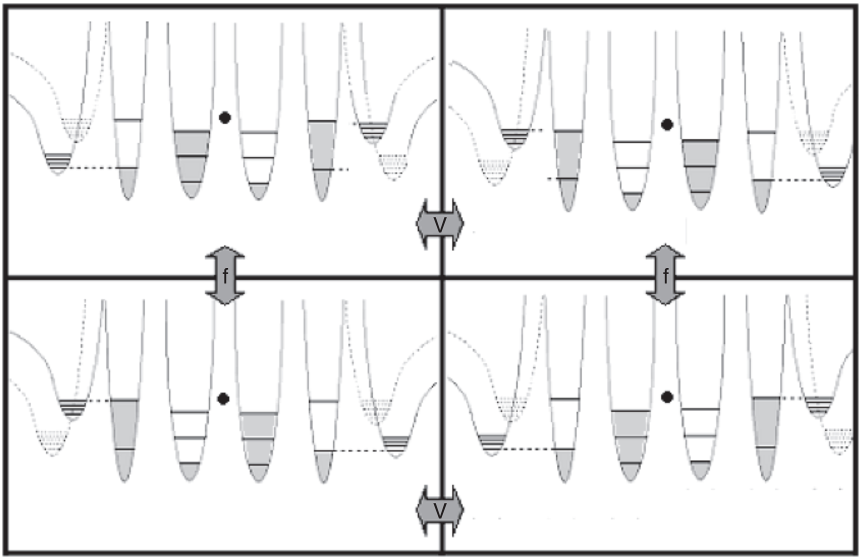

Figure 1.8 Davydov coupling with an unique Fermi resonance. Source: Henri-Rousseau and Blaise 2008 [18]/John Wiley & Sons.

As a consequence, the Hamiltonian of the dimer involving Davydov coupling, Fermi resonances between the g excited state of the fast mode and the g first harmonics of the bending mode is:

$$\left[\mathbb{H}_{\mathrm{Dav}}^{\mathrm{Fermi}}\right] = \begin{pmatrix} \left[\mathbb{H}_{II}^{\{0\}}\right]_g & 0 & 0 & 0 & 0 \\ 0 & \left[\mathbb{H}_{\mathrm{Fermi}}^{\{1\}}\right]_g & 0 & 0 & 0 \\ 0 & 0 & \left[\mathbf{H}_{II}^{\{0\}}\right]_u & 0 & 0 \\ 0 & 0 & 0 & \left[\mathbf{H}_{(+)}^{\{1\}}\right]_u & 0 \\ 0 & 0 & 0 & 0 & \left[\mathbf{H}_{(-)}^{\{1\}}\right]_u \end{pmatrix}$$

Now, proceed as to the corresponding situation when Fermi resonance is not taken into account, it is possible to obtain the spectral density of the present system.

1.2.2 The Spectral Density

The transition dipole moment may be, without and with the electrical anharmonicity, given by:

Without electrical anharmonicity: $\mu\left(\mathbf{q}\right) = \mathbf{q}$

With electrical anharmonicity: $\mu\left(\mathbf{q}, \mathbf{Q}\right) = \mathbf{q}\left(1 + \zeta\mathbf{Q}\right)$

in which ζ is the electrical anharmonicity parameter.

When ignoring the electrical anharmonicity, the ACFs for the IR and the Raman absorptions may be given respectively by

$$\mathbf{G}_{\mathrm{Dav}}(t)^{(u)} = \mathbf{tr}_{\mathrm{Dav}}\left[\rho_{\mathrm{Dav}}\left[\mu(0)_u\right]^{\dagger}\left[\mu(t)_u\right]\right]\text{for pure IR}$$

$$\mathbf{G}_{\mathrm{Dav}}(t)^{(g)} = \mathbf{tr}_{\mathrm{Dav}}\left[\rho_{\mathrm{Dav}}\left[\mu(0)_g\right]^{\dagger}\left[\mu(t)_g\right]\right]\text{for pure Raman}$$

At time t the u transition operator is obtained by the Heisenberg transformation involving the above Hamiltonian $\mathbf{H}_{Dav}$:

$$\mu_u(t) = \frac{1}{\sqrt{2}}\mathbf{e}^{i\mathbf{H}_{\mathrm{Dav}}t/\hbar}$$

$$\left[\left(\left(\mu^{\circ}_{b}\right)\left|\{0\}_a\{1\}_b\right\rangle - \left(\mu^{\circ}_{a}\right)\left|\{1\}_a\{0\}_b\right\rangle\right)\left\langle\{0\}_b\{0\}_a\right|\right]\mathbf{e}^{-i\mathbf{H}_{\mathrm{Dav}}t/\hbar}$$

$$\mu_g(t) = \frac{1}{\sqrt{2}}\mathbf{e}^{i\mathbf{H}_{\mathrm{Dav}}t/\hbar}$$

$$\left[\left(\left(\mu^{\circ}_{b}\right)\left|\{0\}_a\{1\}_b\right\rangle + \left(\mu^{\circ}_{a}\right)\left|\{1\}_a\{0\}_b\right\rangle\right)\left\langle\{0\}_b\{0\}_a\right|\right]\mathbf{e}^{-i\mathbf{H}_{Dav}t/\hbar}$$

It may be shown that the ACF takes the form:

$$\left[\mathbf{G}_{\mathrm{Dav}}(t)\right] = [\mathbf{G}(t)]_g\left[\left[\mathbf{G}^{(+)}(t)\right]_u + \left[\mathbf{G}^{(-)}(t)\right]_u\right]\left(\mathbf{e}^{-\gamma^{\circ}t}\right) \tag{1.23}$$

where γ° is the relaxation parameter of the high-frequency mode. Besides, $[\mathbf{G}(t)]_g$ is the ACF of the g part of the system and where appears the damping parameter γ of the H-bond bridge and the function of it $\tilde{\gamma}$. The quantum calculation of the damping is somewhat complex and appears only on the g part of the ACF. Besides, this last ACF and the $\left[\mathbf{G}^{(\pm)}(t)\right]_u$ which are the ACFs corresponding to the u parts, are respectively:

$$
\begin{aligned}
&\mathbf{G}(t)_g = \left(\mu^{\circ}{}_u\right)^2 \mathbf{e}^{i\omega^{\circ} t} \left(\mathbf{e}^{-i2\tilde{\alpha}^{\circ 2}\Omega t}\right)\left(\mathbf{e}^{i\tilde{\alpha}^{\circ 2}\mathbf{e}^{-\tilde{\gamma}t/2}\sin\Omega t}\right)\left[\mathbf{e}^{\tilde{\alpha}^{\circ 2}[\langle n\rangle+1/2](2\mathbf{e}^{-\tilde{\gamma}t/2}\cos(\Omega t)-\mathbf{e}^{-\gamma t}-1)}\right] \\
&\mathbf{G}^{(\pm)}(t)_u = \varepsilon \sum_{\mu}\sum_{n_u} |B^{\pm}_{\mu\ n_u}|^2 e^{-n_u\hbar\Omega\ /k_B T}\ e^{i\omega^{\pm}_{\mu} t}\ e^{-in_u\Omega t} \\
&\left[[1 \pm (-1)^{n_u+1}] + \eta^{\circ}[1 \mp\ (-1)^{n_u+1}]\right]^2 \\
&\left[\mathbf{H}^{\{1\}}_{\pm}\right]_u \left|\ \beta^{(\pm)}_{\mu}\right\rangle = \hbar\omega^{\pm}_{\mu}\ \left|\ \beta^{(\pm)}_{\mu}\right\rangle \quad \text{with} \left|\ \beta^{(\pm)}_{\mu}\right\rangle = \sum_{n_u} B^{\pm}_{n_u\ \mu}\ \left|\ (n)_u\right\rangle \\
&\left[\mathbf{H}^{\{1\}}_{(\pm)}\right]_u = \frac{\mathbf{P}_u^2}{2M} + \frac{M\Omega^2\mathbf{Q}_u^2}{2} + \frac{1}{\sqrt{2}} b\ \mathbf{Q}_u \pm \mathbf{V}^{\circ}\left(\hat{\mathbf{C}}_2\right)_u
\end{aligned}
\tag{1.24}
$$

The lineshape of the H-bonded dimer is then the Fourier transform of the ACF:

$$
\left[\mathbf{I}_{\text{Dav}}(\omega)\right] = \int_{-\infty}^{\infty} \mathbf{G}_{Dav}(t) e^{-i\omega t}\ \left(e^{-\gamma^{\circ} t}\right) \mathrm{d}t \tag{1.25}
$$

$$
\begin{aligned}
&\left[\mathbf{I}^{\pm}_{\text{Dav}}(\omega)\right] \simeq \sum_{m_g}\sum_{n_g}\left[\mathbf{P}_{m_g n_g}\right]\sum_{n_u}\sum_{\mu}\mathbf{e}^{-\lambda n_u}\left[\left[1 \pm (-1)^{n_u+1}\right] + \eta^{\circ}\left[1 \mp (-1)^{n_u+1}\right]\right]^2 \\
&\left|B^{\pm}_{n_u,\mu}\right|^2 \left[\mathbf{I}^{\pm}_{m_g n_g n_u \mu}(\omega)\right]
\end{aligned}
$$

where the components of the above formulas are given as follows:

$$
\left[\mathbf{I}^{\pm}_{m_g n_g n_u \mu}(\omega)\right] \simeq \frac{\gamma_{m_g n_g}}{\left(\omega - \Omega^{\pm}_{m_g n_g n_u \mu}\right)^2 + \left(\gamma_{m_g n_g}\right)^2}
$$

with

$$
\begin{aligned}
&\Omega^{\pm}_{m_g n_g n_u \mu} = \omega^{\circ} - \left[\left(m_g - n_g + n_u\right)\Omega - \omega^{\pm}_{\mu}\right] - 2\ \tilde{\alpha}^{\circ 2}\Omega \\
&\gamma_{m_g n_g} = \left(m_g + n_g\right)\tilde{\gamma} + \gamma^{\circ} \ \text{ with } \ \tilde{\gamma} = \gamma\sqrt{2} \\
&\left[\mathbf{P}_{m_g n_g}\right] = \frac{\left[1 + \langle n\rangle\right]^{n_g}\tilde{\alpha}^{\circ 2\left(m_g+n_g\right)}}{m_g!n_g!} \\
&\tilde{\alpha}^{\circ} = \frac{\alpha^{\circ}}{\sqrt{2}}, \quad \langle n\rangle = \frac{1}{e^{\tilde{\lambda}} - 1}, \quad \text{and} \quad \tilde{\lambda} = \frac{\hbar\Omega}{k_B T}
\end{aligned}
$$

1.3 Comparison with Experiments

1.3.1 Carboxylic Acid Dimers Ignoring Fermi Resonances

1.3.1.1 Gaseous and Liquid Acetic Acid Dimers

In 2005 [1], it has been proposed an approach of the lineshape in which was introduced the quantum theory of the lineshapes of H-bonded cyclic dimers. This approach was applied to gaseous and liquid acetic acid dimers [19].

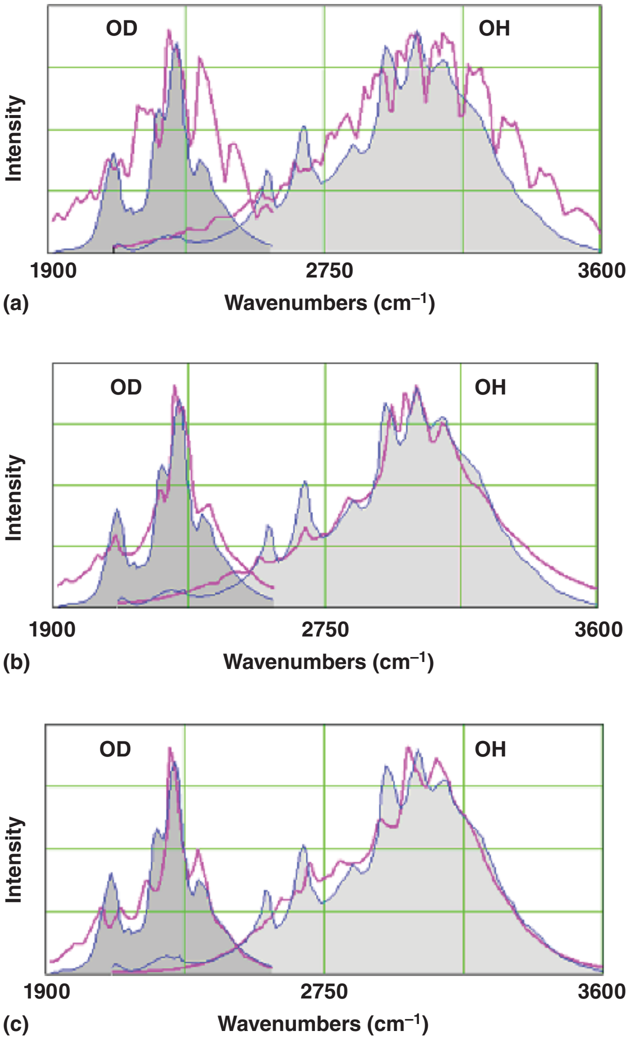

Figure 1.9 IR ν_{XH} lineshapes of gaseous cyclic acetic acid CD_3CO_2H/D dimers at room temperature. Experimental lineshapes (grayed) of Novak and coworker [20].

Figure 1.9 reproduces the corresponding lineshapes involved in the spectra for cyclic CD_3CO_2H/D dimers in the gas phase at room temperature.

The corresponding data are given in Table 1.3.

Moreover, the comparison for the experimental lineshapes dealing with CH_3CO_2H in the gas and liquid phase measured by Flakus and the corresponding theoretical ones [21] resulting from Eq. (1.25) are given in Figure 1.10.

1.3.1.2 Gaseous Acrylic and Propynoic Acids

Now, Figure 1.11a,b compares the experimental lineshapes of O–H and O–D gaseous acrylic and propynoic acids as measured by Bournay and Maréchal [22] to the corresponding theoretical results of [21].

Table 1.3 Parameters used for fitting the experimental lineshapes of Figure 1.9.

Case	Isotope	ω°(cm^{-1})	Ω (cm^{-1})	α°	$\gamma^\circ(\Omega)$	$\gamma(\Omega)$	$V^\circ(\Omega)$	η°
(a)	O–H	3320	108	1.414	0.15	0	−1.10	0
	O–D	2317	98	0.95	0.15	0	−0.96	0
(b)	O–H	3320	108	1.414	0.15	1.10	−1.10	0
	O–D	2317	98	0.95	0.15	1.10	−0.96	0
(c)	O–H	3100	88	1.19	0.20	0.20	−1.50	0.30
	O–D	2263	80	0.77	0.15	0.20	−1.15	0.20

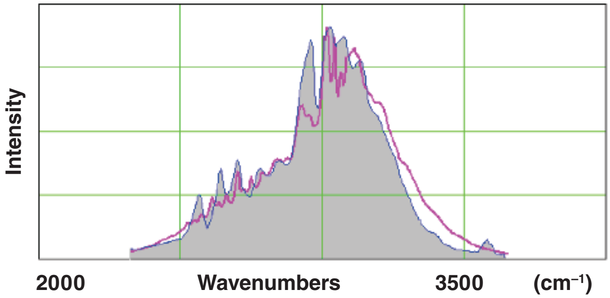

Liquid phase

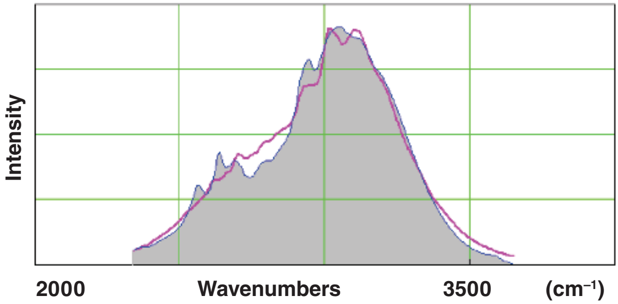

Gas phase

Figure 1.10 Gas and liquid $\nu(X-H)$ *IR* lineshapes of CH_3CO_2H at room temperature. Comparison with experiment. Data are given in Table 1.4. Source: Benmalti et al. [21], figure 1 (p. 272)/With permission of Elsevier.

1.3.2 Carboxylic Acids Taking Into Account Fermi Resonances

1.3.2.1 Crystalline Adipic Acid

In this section, we consider the lineshapes of O–H and O–D crystalline adipic acid. Figure 1.12 gives the comparisons of the experimental lineshapes measured by Auvert and Maréchal [23] of –OH and –OD crystalline adipic acids at different temperatures with the corresponding theoretical ones where Fermi resonances are absent (a) or present (b) in the model [21]. Effect of the η parameter is also shown.

Table 1.4 Parameters used for fitting the experimental lineshapes of acetic acid given in Figure 1.10.

	$\omega^\circ(\text{cm}^{-1})$	$\Omega(\text{cm}^{-1})$	α°	$\gamma^\circ(\Omega)$	$\gamma(\Omega)$	$V^\circ(\Omega)$	η°
Liquid	3100	88	1.19	0.10	0.24	−1.55	0.15
Gas	3100	88	1.19	0.24	0.24	−1.55	0.25

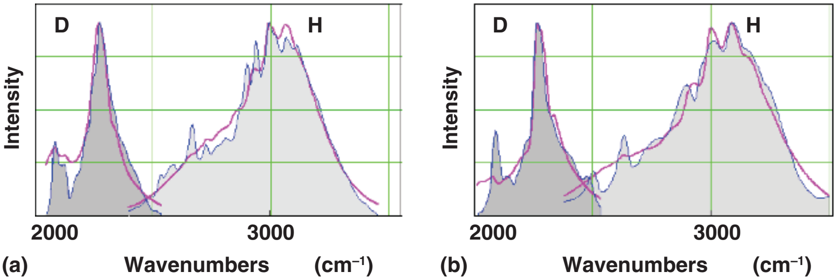

Figure 1.11 Gaseous acrylic (a) and propynoic acids. Comparisons of experimental (grayed) and theoretical lineshapes for H and D isotopic species. Experiment (grayed). The data are given in Table 1.5. Source: Based on Bournay and Maréchal [22].

Table 1.5 Parameters used for fitting the experimental lineshapes of Figure 1.11.

Case	Isotope	$\omega^\circ(\text{cm}^{-1})$	$\Omega(\text{cm}^{-1})$	α°	$\gamma^\circ(\Omega)$	$\gamma(\Omega)$	$V^\circ(\Omega)$	η°
(a) Acrylic acid	O–H	3020	71	1.09	0.22	0.27	−1.66	0.19
	O–D	2237	71	0.77	0.24	1.80	−1.08	0.15
(b) Propynoic acid	O–H	3032	86	1.25	0.27	0.36	−1.94	0.16
	O–D	2260	86	0.88	0.18	1.40	−1.25	0.05

1.3.2.2 Crystalline Polarized and Unpolarized Glutaric Acid Taking Into Account Fermi Resonances

Figure 1.13 compares theoretical and experimental lineshapes of O–H and O–D crystalline glutaric acid as measured by Flakus and Miros [24] at 298 and 77 K for two different polarizations, taking or not into account Fermi resonances.

Now, in presence of Fermi resonances, the theoretical lineshapes may be improved (see Figure 1.14).

The corresponding parameters are given in **Table 1.9 a and b**.

1.3.2.3 Crystalline Thiopheneacetic Acid and Thiopheneacrylic Acids

Rekik et al. [31], have theoretically studied within the standard model, the lineshapes of crystalline thiopheneacetic acid and thiopheneacrylic acids by taking into account the coordinate dependence Θ of the Davydov coupling on slow mode coordinates, and has compared their results to the experimental ones measured by Flakus and Chelmecki [25] in the case where there the polarization is zero.

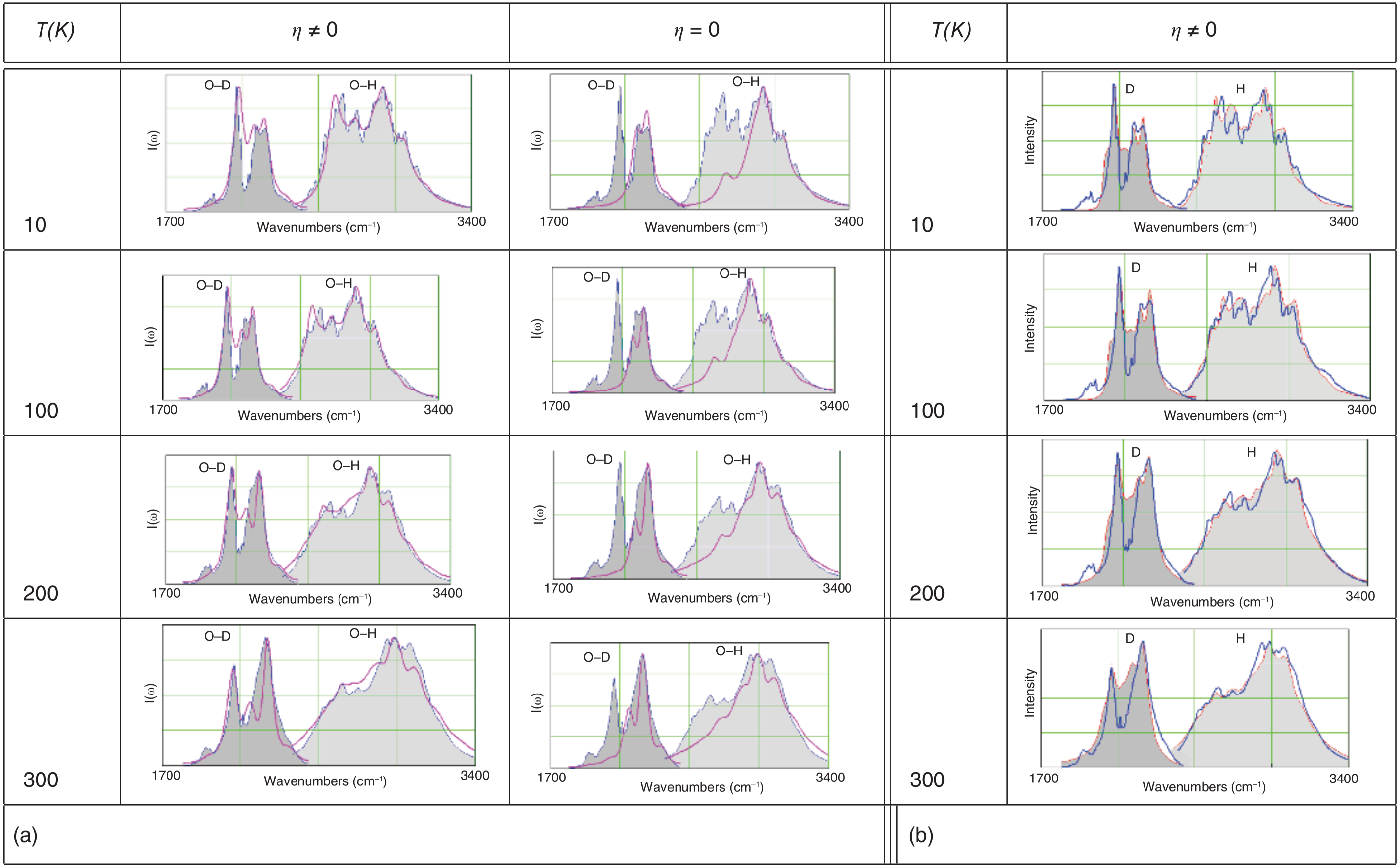

Figure 1.12 Effects of temperature, isotopic substitution, and η parameter on the lineshapes of crystalline adipic acid (a) without Fermi resonance (b) with 4 Fermi resonances. Experiment (grayed). Theory (continuous line). The data are in Tables 1.6 and 1.7a,b. Source: Based on [23].

Table 1.6 Parameters used for fitting the experimental lineshapes of crystalline adipic acid given in Figure 1.12a.

Case	$T(K)$	$\omega°(\text{cm}^{-1})$	Ω (cm^{-1})	$\alpha°$	$\gamma°(\Omega)$	$\gamma(\Omega)$	$V°(\Omega)$	$\eta°$
O–H	10	2990	115	1.00	0.40	0.00	−0.88	0.80
	100	2970	115	1.00	0.40	0.00	−0.88	0.70
	200	2990	115	1.00	0.33	0.20	−0.88	0.50
	300	3020	115	1.00	0.33	0.40	−0.88	0.41
O–D	10	2199	115	0.39	0.22	0.00	−0.54	0.95
	100	2199	115	0.39	0.22	0.00	−0.54	0.95
	200	2203	115	0.39	0.20	0.20	−058	0.85
	300	2199	115	0.35	0.20	0.40	−0.68	0.75

Table 1.7a Parameters used for fitting the experimental lineshapes of Figure 1.12b. in presence of Fermi resonances.

case	T(K)	$\omega°(\text{cm}^{-1})$	Ω (cm^{-1})	$\alpha°$	$\gamma°(\Omega)$	$\gamma(\Omega)$	$V°(\Omega)$	$\eta°$
O–H	10	2865	108	0.88	0.11	0.16	−0.88	0.80
	100	2850	108	0.88	0.11	0.18	−0.88	0.70
	200	2870	108	0.88	0.10	0.34	−0.89	0.50
	300	2890	108	0.88	0.12	0.30	−0.93	0.41
O–D	10	2170	108	0.29	0.22	0.00	−0.54	0.95
	100	2170	108	0.29	0.22	0.10	−0.54	0.95
	200	2170	108	0.29	0.20	0.20	−058	0.85
	300	2172	108	0.29	0.20	0.35	−0.68	0.75

Table 1.7b Fermi resonances parameters for crystalline adipic acid in presence of Fermi resonances given in Figure 1.12b.

Case	T (K)	$f_1^{\bar{v}}$ (cm^{-1})	$f_2^{\bar{v}}$ (cm^{-1})	$f_3^{\bar{v}}$ (cm^{-1})	$f_4^{\bar{v}}$ (cm^{-1})	$\Delta_1^{\bar{v}}$ (cm^{-1})	$\Delta_2^{\bar{v}}$ (cm^{-1})	$\Delta_3^{\bar{v}}$ (cm^{-1})	$\Delta_4^{\bar{v}}$ (cm^{-1})	$\gamma_1^{\bar{v}}$ (Ω)	$\gamma_2^{\bar{v}}$ (Ω)	$\gamma_3^{\bar{v}}$ (Ω)	$\gamma_4^{\bar{v}}$ (Ω)
O–H	10 100 200 300	30	37	36	36	−155	−80	20	220	0.10	0.10	0.10	0.05
O–D	10 100 200 300	17	15	13	13	−33	−21	−0.84	126	0.07	0.04	0.17	0.10

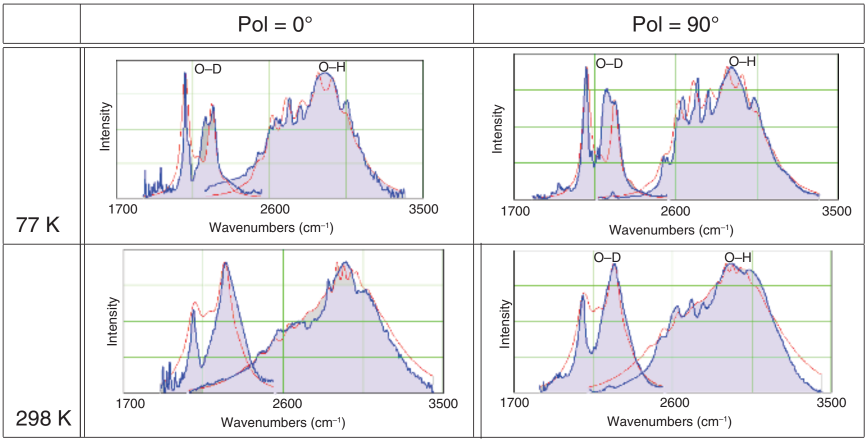

Figure 1.13 Temperature and isotopic substitution effects at different polarizations for crystalline glutaric acid without Fermi resonances. Grayed: Experimental lineshapes of Flakus and Miros [24].

Table 1.8 Parameters used for fitting the experimental lineshapes of Figure 1.13 of crystalline glutaric acid without Fermi resonance.

Pol (°)	Case	T(K)	$\omega°(\text{cm}^{-1})$	Ω (cm^{-1})	$\alpha°$	$\gamma°(\Omega)$	$\gamma(\Omega)$	$V°(\Omega)$	$\eta°$
0	O–H	77	3123	85	1.50	0.40	0.10	−1.20	0.60
	O–H	298	3123	85	1.50	0.15	0.90	−1.20	0.20
	O–D	77	2203	85	0.38	0.30	0.10	−0.85	1.30
	O–D	298	2203	85	0.38	0.50	0.20	−0.85	0.60
90	O–H	77	3123	85	1.50	0.40	0.10	−1.20	0.75
	O–D	298	3123	85	1.50	0.15	0.90	−1.20	0.30
	O–H	77	2208	85	0.38	0.30	0.10	−0.85	1.30
	O–D	298	2208	85	0.38	0.20	0.20	−0.85	0.70

Crystalline Thiopheneacetic Acid For the crystalline thiophene acetic acid they have found the spectra given in Figure 1.15.

The corresponding parameters are given in Table 1.10.

Crystalline H(D)-3-Thiopheneacrylic Acid For the crystalline H(D)-3-thiopheneacrylic acid they obtained the results given in Figure 1.16. (Table 1.11)

The corresponding parameters are given in Table 1.11.

1.3.2.4 l.2-Naphtylacetic Acid (2-NA) Crystals

In this chapter, Ghalla and coworkers [26] presents results of a theoretical study on ν_s (O–H(D)) band shapes in the polarized IR spectra of 2-naphtylacetic acid (2-NA) crystals measured at the temperature of liquid nitrogen, based on our original theory.

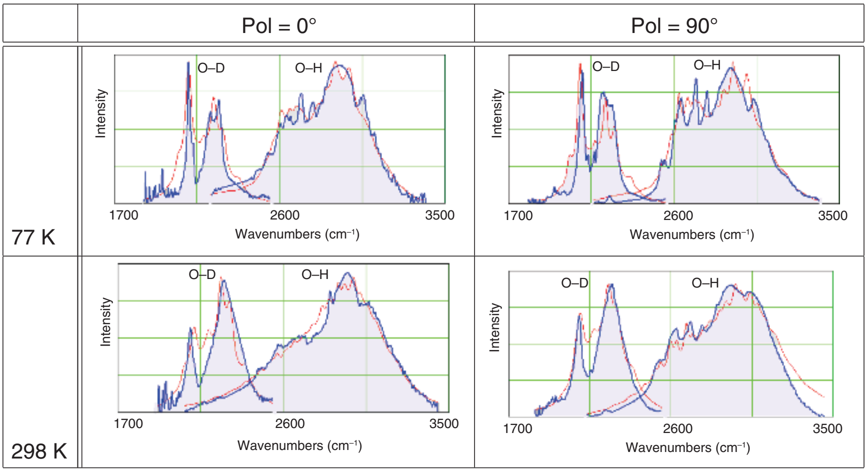

Figure 1.14 Temperature and isotopic substitution effects at different polarizations for crystalline glutaric acid with Fermi resonances. Grayed: Experimental lineshapes of Flakus and Miros [24]. Source: Based on Flakus and Miros [24].

Table 1.9a Parameters used for fitting the experimental lineshapes of crystalline glutaric in presence of Fermi resonance, given in Figure 1.14.

Pol (°)	**Case**	T **(K)**	$\omega°(\mathrm{cm}^{-1})$	$\Omega\ (\mathrm{cm}^{-1})$	$\alpha°$	$\gamma°(\Omega)$	$\gamma(\Omega)$	$V°(\Omega)$	$\eta°$
	O–H	77	3063	90	1.50	0.20	0.10	−115	0.55
0	O–H	298	3063	90	1.50	0.15	0.20	−1.15	0.12
	O–D	77	2202	90	0.38	0.15	0.20	−0.82	1.00
	O–D	298	2217	90	0.38	0.10	0.20	−0.82	0.40
	O–H	77	3083	90	1.50	0.20	0.20	−1.15	0.70
0	O–D	298	3083	90	1.50	0.25	0.25	−1.15	0.40
	O–H	77	2188	90	0.38	0.20	0.20	-0.82	1.00
	O–D	298	2217	90	0.38	0.25	0.25	−0.82	0.50

The line shapes were studied within the frameworks of our original theory of strong anharmonic coupling, Davydov coupling, Fermi resonance coupling, direct and indirect damping, and a selection rule breaking mechanism for forbidden transitions in IR.

The present approach (see Figure 1.17) correctly fits the experimental line shape of the hydrogenated compound and predicts satisfactorily the evolution in the lineshapes with isotopic substitution. Numerical calculations show that mixing of all these effects allows one to reproduce satisfactorily the main features of the experimental IR lineshapes of hydrogenated and deuterated 2-NA crystals and is expected to confirm the importance of the Fermi resonances in reproducing the experimental spectra. Parameters are given in Tables 1.12 and 1.13.

Table 1.9b (continued). Fermi resonances parameters for crystalline glutaric acid (cf. Figure 1.14).

Pol	**Case**	***T* (K)**	$f_1^{\bar{v}}$	$f_2^{\bar{v}}$	$f_3^{\bar{v}}$	$f_4^{\bar{v}}$	$f_5^{\bar{v}}$	$\Delta_1^{\bar{v}}$	$\Delta_2^{\bar{v}}$	$\Delta_3^{\bar{v}}$	$\Delta_4^{\bar{v}}$	$\Delta_5^{\bar{v}}$	$\gamma_1^{\bar{v}}$	$\gamma_2^{\bar{v}}$	$\gamma_3^{\bar{v}}$	$\gamma_4^{\bar{v}}$	$\gamma_5^{\bar{v}}$
			(cm^{-1})	(cm^{-1})	(cm^{-1})	(cm^{-1})	(cm^{-1})	(cm^{-1})	(cm^{-1})	(cm^{-1})	(cm^{-1})	(cm^{-1})	(Ω)	(Ω)	(Ω)	(Ω)	(Ω)
	O–H	77															
0	O–H	298	40	25	20	30	30	−430	−120	30	100	200	0.10	0.10	0.10	0.10	0.10
	O–D	77															
	O–D	298															
	O–H	77		23									0.05	0.05	0.05	0.05	0.05
90	O–H	298	40	0	20	30	30	−430	−430	30	310	200	0.10	0.10	0 10	0.10	0.10
	O–D	77		25									0.10	0.10	0.10	0.10	0.10
	O–D	298		0									0.10	0.10	0.10	0.10	0.10

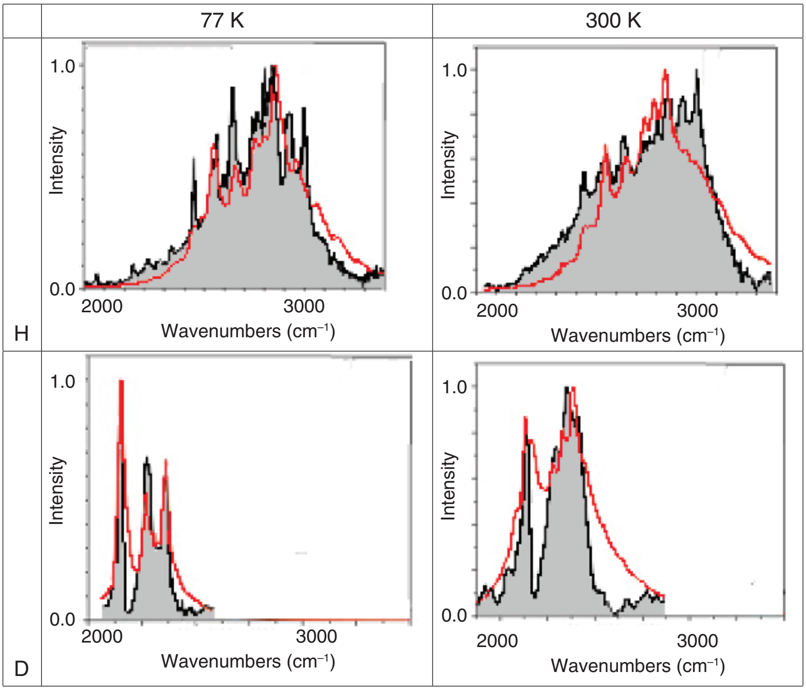

Figure 1.15 Crystalline H(D)-3-thiophenacrylic acid experimental (H-3TAcetic) (grayed) and theoretical lineshapes at different temperatures and H/D isotopic species. Source: Modified from Rekik et al. 2015 [31].

Table 1.10 Parameters used for fitting the experimental lineshapes of the 3-thiopheneacetic (H-3TAcetic) acid crystals dimers and their deuterated analogs (Pol = 0).

Species	T (K)	$\omega°(\text{cm}^{-1})$	$\Omega(\text{cm}^{-1})$	$\alpha°$	$\gamma°(\Omega)$	$\gamma(\Omega)$	$VD°(\Omega)$	Θ
H-3TAcetic	77	3180	105	1.55	0.35	0.35	0.50	0.15
H-3TAcetic	300	3050	105	1.2	0.3	0.25	1.2	0.22
D-3TAcetic	77	2250	80	0.67	0.15	0.25	0.52	0.2
D-3TAcetic	300	2250	85	0.63	0.17	0.25	0.7	0.2

1.3.2.5 Crystalline Aspirin Dimers Involving Slow Mode Morse Potential

The application of our treatment for Davydov coupling has been performed with aspirin by Rekik and coworkers [27] by accounting for the anharmonicity of the slow mode which is described by a “Morse” potential with a dissociation energy of $D_e = 2100\,\text{cm}^{-1}$ to reproduce the polarized IR spectra of the hydrogen and deuterium bond in acetylsalicylic acid (aspirin) crystals.

Within the adiabatic approximation, the Hamiltonian of each moiety of the dimer may be put on the form of sum of effective Hamiltonians which are depending on the degree of excitation of the fast mode.

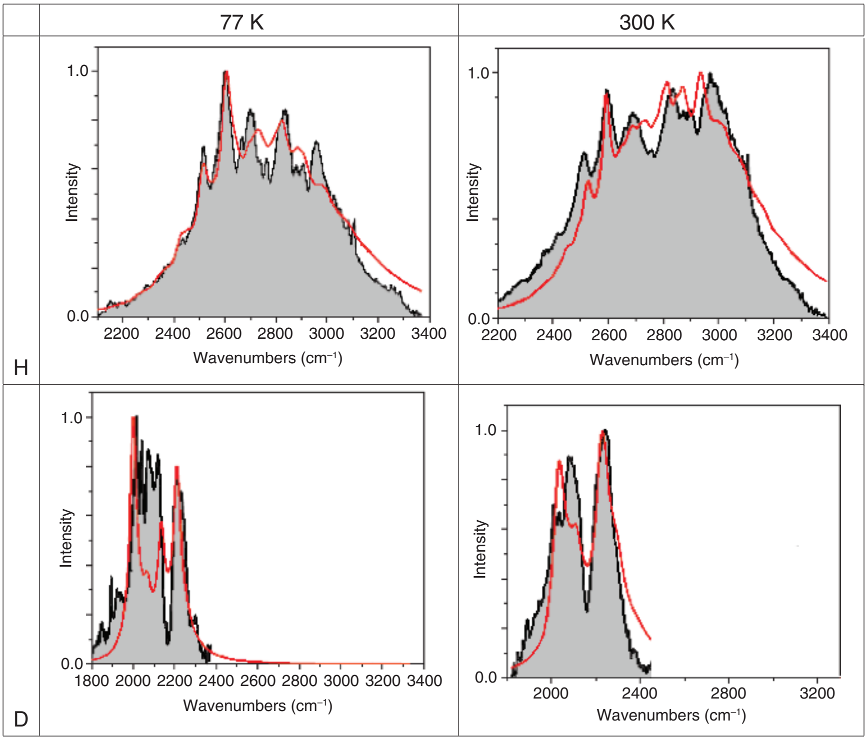

Figure 1.16 Crystalline H(D)-3-thiophenacrylic acid experimental (black line); theoretical (red line) lineshapes at different temperatures for H and D isotopic species. Source: Rekik et al. 2015 [31]/With permission of Elsevier.

Table 1.11 Parameters used for fitting the experimental lineshapes of the crystalline 3-thiopheneacrylic (H-3TAcrylic) acid dimers and their deuterated analogs.

Pol = 0	T (K)	$\omega°(\mathrm{cm}^{-1})$	$\Omega(\mathrm{cm}^{-1})$	$\alpha°$	$\gamma°(\Omega)$	$\gamma(\Omega)$	$VD°(\Omega)$	Θ
H-3TAcrylic	77	2950	85	1.1	0.3	0.3	0.9	0.23
H-3TAcrylic	300	3020	85	1.23	0.3	0.15	1	0.23
D-3TAcrylic	77	2125	75	0.65	0.22	0.2	0.65	0.12
D-3TAcrylic	300	2150	75	0.63	0.24	0.25	0.65	0.4

These corrections are introduced in the usual procedure for taking into account the Davydov coupling. The theoretical lineshapes obtained are compared to the experimental ones obtained by these authors for the two isotopic species at 77 and 300 K temperatures. Their results are given in Figure 1.18 and the coresponding parameters in Table 1.14.

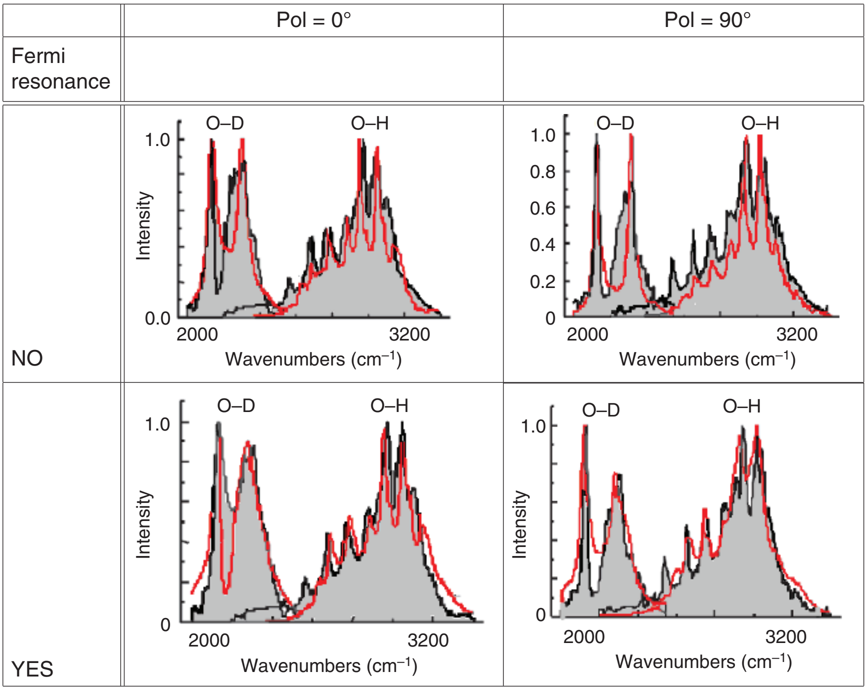

Figure 1.17 2-Naphtylacetic Acid (2-NA). Comparison of experimental lineshapes with theoretical ones for different polarizations and isotopic substitutions, without and with 3 Fermi resonances. Source: Issaoui et al. 2013 [26]/ Springer Nature.

Table 1.12 Parameters used to fit experimental H/D-2-NA spectra.

Species	Pol(°)	$\omega°\,(\mathrm{cm}^{-1})$	$\Omega\,(\mathrm{cm}^{-1})$	$\alpha°$	$\gamma°(\Omega)$	$\gamma(\Omega)$	$V°(\hbar\Omega)$	η
–H	0	3135	67	1.56	0.20	0.05	−1.55	0.45
–H	90	3110	65	1.60	0.22	0.002	−1.65	0.20
–D	0	2221	90	0.364	0.30	0.10	−0.857	0.98
–D	90	2221	90	0.364	0.17	0.10	−1.00	0.98

1.3.2.6 Phthalic and Terephthalic Acid Crystals

Phthalic (PAC) and terephthalic (TAC) acid crystals have been studied by Rekik et al. [36].

They have studied two interacting cyclic dimers shown in Figure 1.19 in which the q_i and Q_i are respectively the fast and slow modes position coordinates while $V°_{D_1}$ and $V°_{D_2}$ are the Davydov coupling involved in each system of the superdimer. They have considered the full Hamiltonian of the superdimer for its diagonal part as the

Table 1.13 Values of Fermi coupling parameters used for fitting experimental H/D-2-NA spectra.

Pol(°)	f_1(cm^{-1})	f_2(cm^{-1})	f_3(cm^{-1})	Δ_1(cm^{-1})	Δ_2(cm^{-1})	Δ_3(cm^{-1})	$\gamma_{\Delta_1}(\Delta_1)$	$\gamma_{\Delta_2}(\Delta_2)$	$\gamma_{\Delta_3}(\Delta_3)$
–H 0	10	10	20	60	–80	42	0.4	0.4	10
–H 90	20	10	10	110	120	150	0.2	0.2	0.2
–D 0	20	30	30	140	110	–180	0.2	0.2	0.2
–D 90	20	30	30	140	110	–180	0.2	0.2	0.2

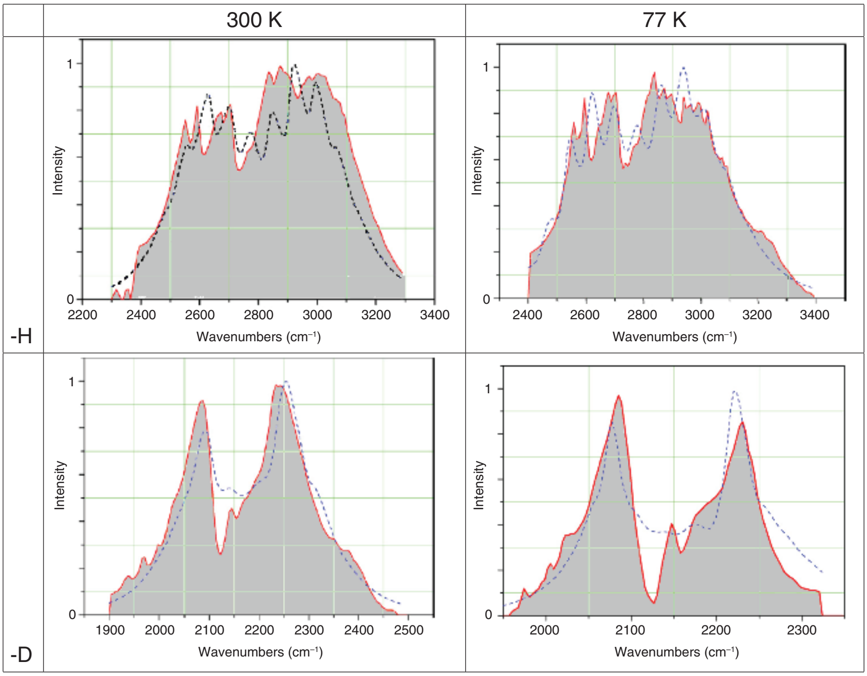

Figure 1.18 Comparison between the experimental (grayed) and theoretical (dashed line) spectra for Aspirin-H (polycrystalline acetylsalicylic acid) at 300 and 77 K. Source: Ghalla et al. 2010 [27]/ With permission of Elsevier.

Table 1.14 Parameters used for fitting experimental Aspirin-H and Aspirin-D acid dimer spectra.

Compound	T(K)	$\omega°$(cm^{-1})	Ω(cm^{-1})	$\alpha°$	$V°$	$\gamma°(\Omega)$	$\gamma(\Omega)$	η
Aspirin-H	300	2910	76	0.95	−1.75	0.25	0.1	0.85
Aspirin-H	77	3095	77	1.62	−1.70	0.35	0.1	0.8
Aspirin-D	300	2185	86	0.743	−1.69	0.25	0.7	0.7
Aspirin-D	77	2228	77	1.238	−1.65	0.25	1.1	0.8

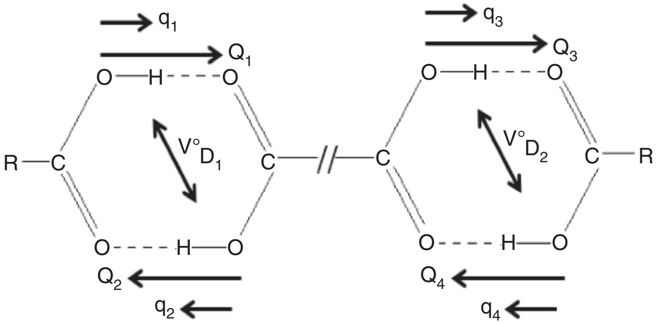

Figure 1.19 Structure of the superdimer and definition of the eight vibrational modes involved in the superdimer dynamics.

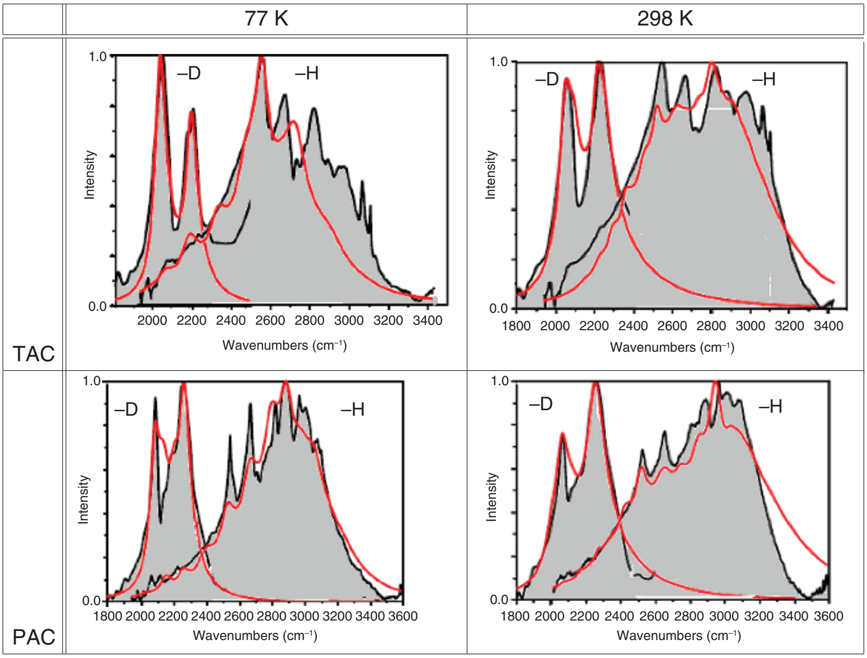

Figure 1.20 Crytalline phthalic (PAC) and terephthalic (TAC) acids at 77 and 298 K. Comparison of experimental (grayed) and theoretical (full line) lineshape. Source: Based on Rekik et al. 2020 [36].

sum of the diagonal parts of each component and as for its off parts as the sum of the Davydov couplings of each component. Their results are shown in Figure 1.20 for the H6 and D6 isotopomers of Phthalic (PAC) and terephthalic (TAC) acid crystals using the parameters given in Table 1.15.

1.3.2.7 Liquid Formic Acid Mixing of Monomer and Dimer

A full quantum-theoretical approach has been used by Fathi et al. [28] to study the mOAH experimental IR lineshapes of liquid formic acid. For this purpose, the

Table 1.15 Theoretical parameters used for the fitting of the experimental lineshapes of PAC and TAC.

Cases	T(K)	$\omega^\circ{}_{D_1}$ (cm $^{-1}$)	$\alpha^\circ{}_{D_2}$ (cm $^{-1}$)	Ω_{D_1} (cm $^{-1}$)	$\Omega{}_{D_2}$ (cm $^{-1}$)	α	κ	$\gamma^\circ(\omega^{\circ\circ}{}_{D_1})$	$V^\circ{}_{D_1}(\Omega_{D_1})$	$V^\circ{}_{D_2}(\Omega_{D_2})$
D6 PAC	77	2180	2193	69	62	0.85	0.95	0.32	0.84	0.8
D6 PAC	298	2150	2167	64	60	0.96	0.87	0.31	1.29	1.35
D6 TAC	77	2130	2142	70	66	1.15	1.04	0.27	1.76	1.8
D6 TAC	298	2130	2119	62	65	1.02	1.13	0.25	1.83	1.8
H6 PAC	77	3200	3188	68	61	1.26	1.36	0.37	0.68	0.6
H6 PAC	298	3050	3012	64	71	1.45	1.39	0.34	1.02	1.06
H6 TAC	77	2860	2895	66	68	1.49	1.57	0.24	1.06	1.10
H6 PTAC	298	2850	2887	63	65	1.52	1.48	0.28	1.46	1.41

Table 1.16 Parameters used in the theoretical fitting of formic acid species.

Species	ω°(cm^{-1})	Ω(cm^{-1})	α°	$V^\circ{}_D$	$\gamma^\circ(\Omega)$	$\gamma(\Omega)$	η	r
HCOOH	3030	95	1.4	−1.2	0.5	0.1	0.0	0.25
HCOOD	2340	110	0.85	−1.0	0.5	0.1	0.3	0.12
DCOOH	3080	95	1.5	−1.2	0.7	0.03	0.1	0.15
DCOOD	2240	110	0.62	−0.75	0.3	0.02	0.08	0.25

authors use our original theory, based on the strong anharmonic coupling between the high-frequency mode and the H-bond bridge, and including the Davydov coupling between the excited states of the two moieties, multiple Fermi resonances between the mOAH (Bu) mode and combinations of some bending modes, together with the quantum direct and indirect dampings. They have studied the influence of the proportion of dimers species with respect to monomers to obtain the best fitting with experimental spectra. This model reproduces satisfactorily the main features of the experimental lineshapes of liquid hydrogenated and deuterated formic acid, by using a minimum set of independent parameters as it may be seen in Figure 1.21.

In Tables 1.16 and 1.17 are given the parameters used in the calculation. r is the ratio Dimer/Monomer. The other parameters are those used in our original theory.

Parameters used to reproduce the experimental spectra of HCOOH and its deuterated derivatives DCOOH, HCOOD, and DCOOD of Figure 1.21.

1.3.2.8 Crystalline Furoic Acid Dimer with Slow Mode Morse Potential and Fermi Resonances

Ghalla et al. [29], have compared the experimental IR lineshapes of polarized crystalline Furoic acid dimers [30] at 77 K with their theoretical ones calculated

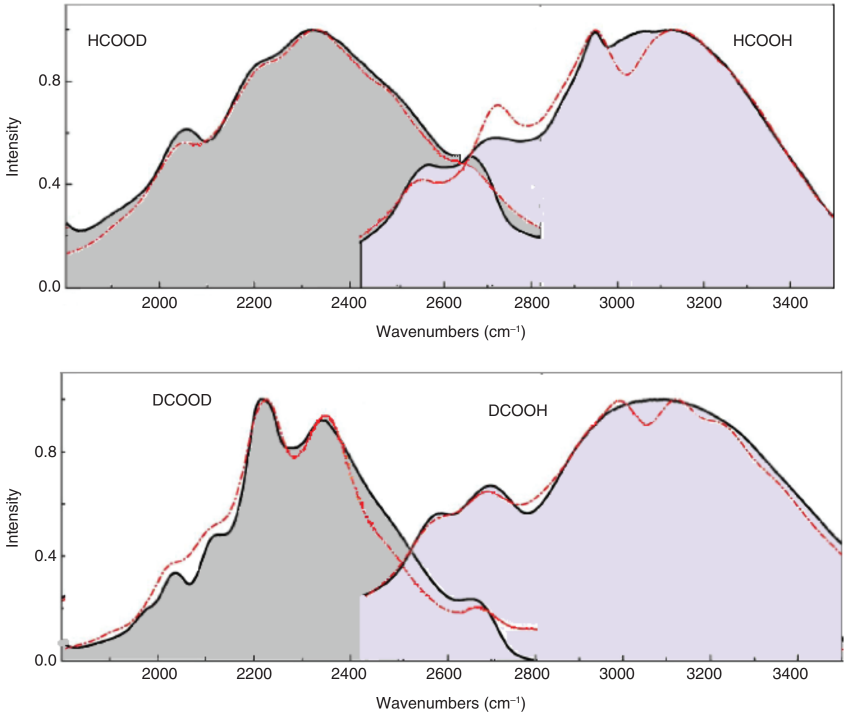

Figure 1.21 Liquid formic acid mixing of monomer and dimer of several H/D species. Experiment: grayed: Dashed red: theory. The corresponding parameters are given in Tables 1.16 and 1.17. Source: Modified from Fathi et al. 2017 [28].

Table 1.17 Fermi resonances parameters for crystalline glutaric acid (cf. Figure 1.14.

Species	f_1 (cm^{-1})	f_2 (cm^{-1})	f_3 (cm^{-1})	f_4 (cm^{-1})	ω_1 (cm^{-1})	ω_2 (cm^{-1})	ω_3 (cm^{-1})	ω_4 (cm^{-1})	γ_{δ_1} (Ω)	γ_{δ_1} (Ω)	γ_{δ_3} (Ω)	γ_{δ_4} (Ω)
HCO_2H	30	85	95	–	3130	2660	2850	–	0.1	0.05	0.02	–
HCO_2D	60	75	75	50	2285	2670	2110	2495	0.01	0.01	0.01	0.01
DCO_2H	–	75	135	–	–	2710	2850	–	–	0.01	0.01	–
DCO_2D	50	30	70	35	2060	2350	2680	2140	0.02	0.2	0.02	0.0

by introducing Morse potential for the slow modes. Their results are given in Figure 1.22.

They have improved the agreement with experiment by introducing in the model 3 Fermi resonances. In both situations, the theoretical lineshapes appear as continuous lines whereas the experimental ones are grayed.

In Figure 1.23 is given the comparison between the experiment (grayed) and theory as computed by Eq. (1.25). The slow modes are described by a Morse potential. The parameters used in the computations are given in Tables 1.18 and 1.19.

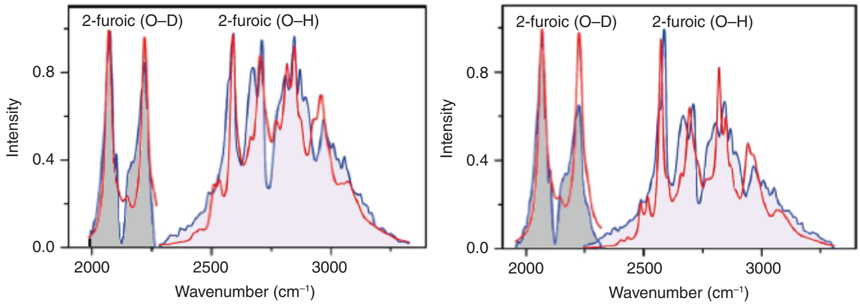

Figure 1.22 Lineshapes of polarized 2-furoic acid when the Fermi resonances are ignored, at 77 K. Source: Ghalla et al. [29]/John Wiley & Sons.

Table 1.18 Parameters involved for fitting the experimental spectra of 2-furoic acid.

Species	Pol(°)	$\omega^\circ\,(\mathrm{cm^{-1}})$	$\Omega\,(\mathrm{cm^{-1}})$	α°	$V^\circ(\hbar\Omega)$	$\gamma^\circ(\Omega)$	$\gamma(\Omega)$
H	0	3030	80	1.45	1.10	0.2	0.1
D	0	2142	90	0.331	0.786	0.15	0.1
H	90	2995	85	1.36	1.13	0.15	0.1
D	90	2144	87	0.318	0.857	0.18	0.1

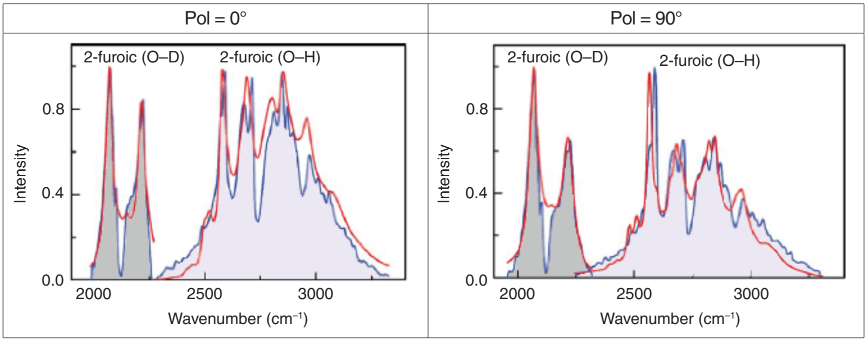

Figure 1.23 Lineshapes of polarized 2-furoic acid when there are three Fermi resonances at 77 K. Source: Ghalla et al. [29]/John Wiley & Sons.

Table 1.19 Fermi coupling parameters (in $\mathrm{cm^{-1}}$) used for fitting experimental 2-furoic acid spectra.

Pol(°)	$f_1(\mathrm{cm^{-1}})$	$f_2(\mathrm{cm^{-1}})$	$f_3(\mathrm{cm^{-1}})$	$\Delta_1(\mathrm{cm^{-1}})$	$\Delta_2(\mathrm{cm^{-1}})$	$\Delta_3(\mathrm{cm^{-1}})$	$\gamma_{\Delta_1}(\Delta_1)$	$\gamma_{\Delta_1}(\Delta_2)$	$\gamma_{\Delta_3}(\Delta_3)$
H 0	95	95	80	30	20	10	0.2	0.2	0.2
D 0	93	105	116	10	10	10	0.2	0.2	0.2
H 90	95	95	100	20	20	10	0.2	0.2	0.2
D 90	83.1	105	106	10	10	10	0.2	0.2	0.2

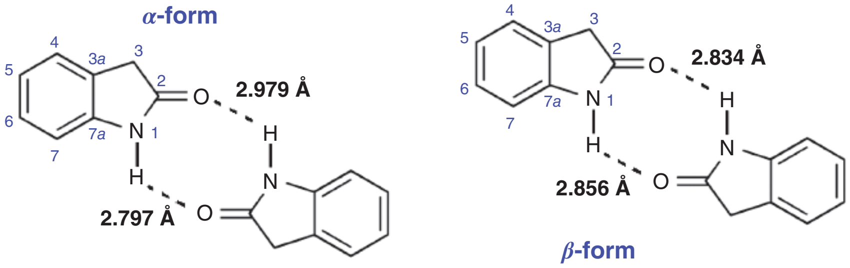

Figure 1.24 The two forms of oxindol.

Table 1.20 Parameters used for fitting the experimental line shapes of the ν_S(N−H) stretching band of (α/β)-hydrogenated and (α/β)-deuterated oxindole complexes at $T = 77$ K and $T = 293$ K.

Compound	T(K)	ω°_1 (cm^{-1})	ω°_2 (cm^{-1})	α_1	α_2	$\Omega_1 = \Omega_2$ (cm^{-1})	$\gamma^\circ(\Omega)$	$V_{Dav}^{HH/DD}$ (cm^{-1})
α-D oxindole	77	2350	2460	0.65	0.726	65	0.37	85.8
β-D oxindole	77	2352	2293	0.50	0.518	67	0.40	93.4
α-D oxindole	293	2350	2475	0.65	0.712	65	0.35	65
β-D oxindole	293	2280	2367	0.70	0.714	65	0.36	91
α- H oxindole	77	3160	3335	1.0	1.230	75	0.39	167.5
β-H oxindole	77	3070	3159	1.0	1.068	70	0.38	179
α-H oxindole	293	3110	3296	1.0	1.160	80	0.40	144
β-H oxindole	293	3120	3230	1.0	1.040	70	0.40	176

1.3.2.9 Other Kinds of H-Bonded Compounds

Combined Crystalline Oxindole Acid Dimers Another application was done by Ghalla et al. on oxindole crystals (2,3-dihydro-1*H*-indol-2-one) which form cyclic dimers with two different H-bonds [34]. In these molecules, we find the group H-N-C=O which is involved in the formation of cyclic dimer of H-bonds (α-form; β-form). They studies 2 forms of oxindol crystal, the α- and the β forms. The oxindole acid molecules form a cyclic, non-centrosymmetric acid dimer with two different H-bond bridges because they have different bond lengths as it is shown in Figure 1.24.

They have introduced for the coupling of the fast mode angular frequency with the slow mode coordinate of the hydogenated and deuterated compounds, a subtil dependence on the slow mode coordinate The consequence is that there are two different coupling parameters. Using the parameters of Table 1.20 the following spectra are given in Figure 1.25.

1.3.2.10 Phosphinic Acid Dimer

Hydrogen-bonded dimers of phosphinic acid (See Figure 1.26) and their deuterated analogs [(R_2POOH(D), with R = CH_2Cl, CH_3], IR lineshapes of phosphinic acids

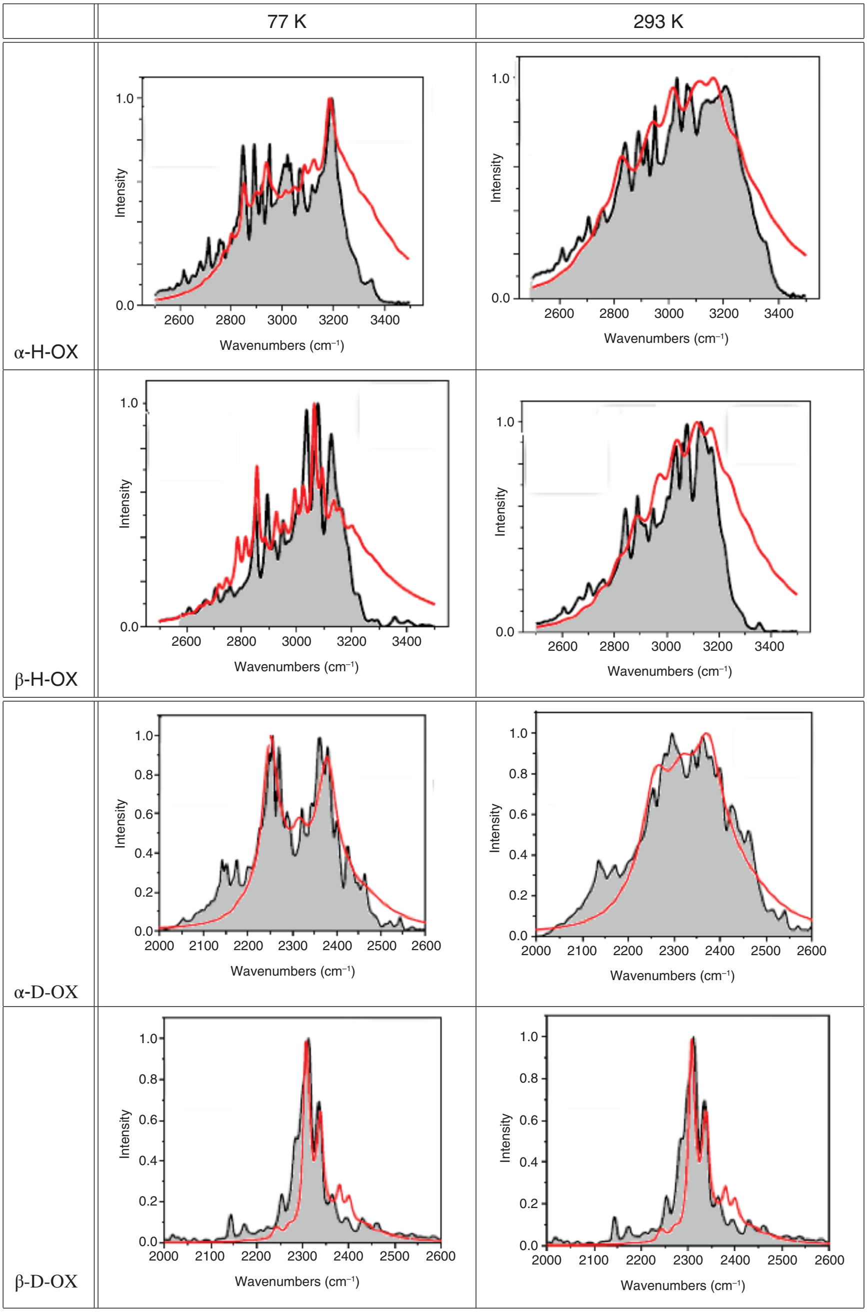

Figure 1.25 Lineshapes of (α/β)-hydrogenated and (α/β)-deuterated oxindole complexes at $T = 77$ K and $T = 293$ K. Grayed: experimental spectra. Source: Rekik et al. 2020 [36] / With permission of Elsevier.

Figure 1.26 Dimer of phosphinic acid.

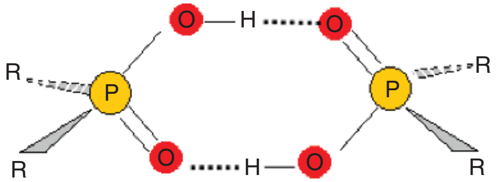

Table 1.21a Parameters used for fitting the experimental lineshapes of $(CH_2Cl)_2PO_2H/D$ and $(CH_3)_2PO_2H/D$.

	T(K)	$\omega°(\text{cm}^{-1})$	$\Omega(\text{cm}^{-1})$	$D_e(\text{cm}^{-1})$	α	$\gamma°(\Omega)$	$\gamma(\Omega)$	$V_D(\Omega)$	η
$(CH_2Cl)_2PO_2H$	435	2300	205	2100	0.80	0.40	0.1	1.68	0.9
$(CH_2Cl)_2PO_2D$	475	1860	202	2100	0.25	0.35	0.1	0.55	0.49
$(CH_3)_2PO_2H$	530	2415	206	2100	0.95	0.55	0.1	1.9	0.6
$(CH_3)_2PO_2D$	515	1880	204	2100	0.30	0.65	0.1	0.78	0.29

R_2PO_2H dimers in the gas phase have been studied by Rekik and Alshammari [32] and compared with experiment [35] (See **Figure** 1.27)

The theoretical model is based on a model for a centrosymmetric hydrogen-bonded dimer that treats the high-frequency OH stretches harmonically and the low-frequency intermonomer (i.e. O· · ·O) stretches anharmonically. This model takes into account the following effects: anharmonic coupling between the OH and O· · ·O stretching modes; Davydov coupling between the two hydrogen bonds in the dimer; promotion of symmetry-forbidden OH stretching transitions; Fermi resonances between the fundamental of the OH stretches and the overtones of the in- and out-of-plane bending modes involving the OH groups; direct relaxation of the OH stretches; and indirect relaxation of the OH stretches via the O· · ·O stretches. Using a set of physically significative parameters into this model, the authors reproduce the main features in the experimental OH(D) bands of these dimers. By increasing the number and strength of the Fermi resonances and by promoting symmetry-forbidden OH stretching transitions in our simulations, they directly see the emergence of the ABC structure, which is a characteristic feature in the spectra of very strongly hydrogen-bonded dimers. However, in the case of the deuterated dimers, which do not exhibit the ABC structure, the Fermi resonances are found to be much weaker.

The parameters corresponding to Figure 1.27 are given in Tables 1.21a and b.

1.3.2.11 Monomer of $(CH_3)_2O\cdots HCl$

Taking Into Account Coupling Between Slow and Bending Modes In a recent paper, Rekik et al. [33] have calculated the IR spectral density of the ν_S $(Cl-\overrightarrow{H})$ band in gaseous $(CH_3)_2O\cdots HCl$ complex in order to fit the experimental spectra obtained by Lassegues and Huong [37]. (See Figure 1.28) They have used a Morse curve for the potential of the slow mode and introduced an additional bending mode effect

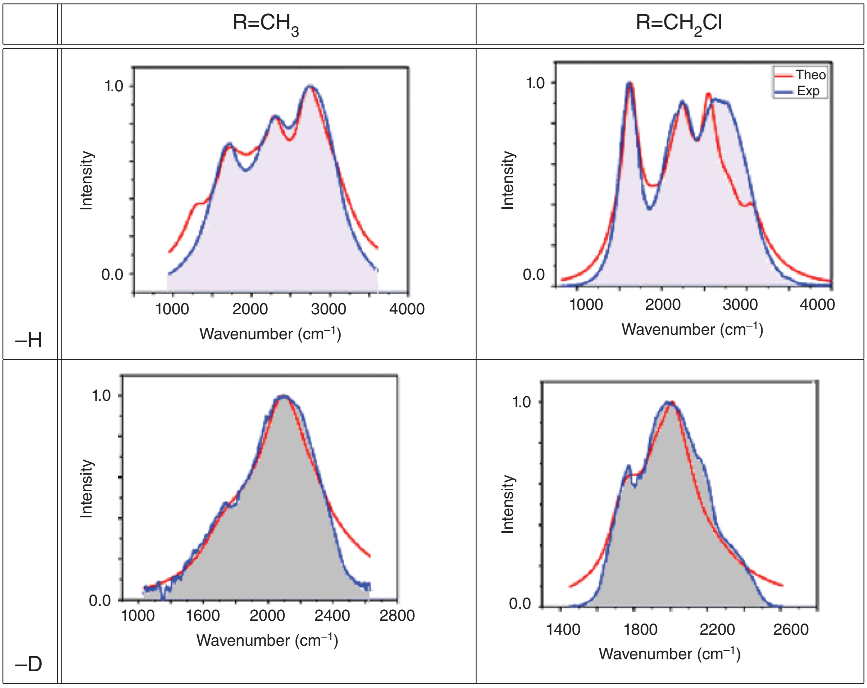

Figure 1.27 Comparison between experimental (grayed) and theoretical lineshapes of dimeric CH_3– and CH_2Cl– phosphinic acids H/D analogs. Source: Rekik et al. 2012 [33]/ American Chemical Society.

Table 1.21b Fermi resonance parameters for used for fitting the experimental lineshapes of $(CH_2Cl)_2PO_2H/D$ and $(CH_3)_2PO_2H/D$ (Continuation of Table 1.21a).

	$\Delta_1(\mathrm{cm}^{-1})$	$\Delta_2(\mathrm{cm}^{-1})$	$f_1(\mathrm{cm}^{-1})$	$f_2(\mathrm{cm}^{-1})$	$\gamma_1^{\delta}(\Omega)$	$\gamma_2^{\delta}(\Omega)$
$(CH_2Cl)_2PO_2H$	380	320	96	120	0.02	0.02
$(CH_2Cl)_2PO_2D$	225	115	30	10	0.02	0.02
$(CH_3)_2PO_2H$	−255	−220	110	120	0.02	0.02
$(CH_3)_2PO_2D$	5	25	15	20	0.02	0.02

for improving the fitting by the theoretical lineshape. This procedure writes the total Hamiltonian of the complex as the sum:the parameter α° and β are the coupling of the fast mode with respectively the slow and bending modes. They have compared their results with the experimental lineshape (grayed) with the parameters given in Table 1.22.

Taking Into Account Electrical Anharmonicity On the same compound, Rekik et al. [16, 17] take into account the electrical anharmonicity and dampings in explaining the IR spectrum of gaseous $(CH3)_2O \cdots HCl$ complex (see Figure 1.29 and corresponding data in Table 1.23).

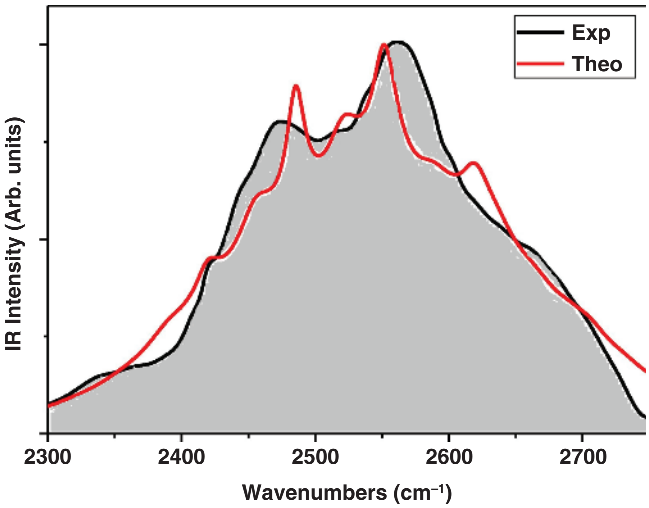

Figure 1.28 $(CH_3)_2$ O· · ·HCl complex in gas phase at 226 K . Source: Rekik et al. 2019 [34]/With permission of Elsevier.

Table 1.22 Parameters used in the theoretical lineshape of Figure 1.28.

$\omega°(cm^{-1})$	$\Omega(cm^{-1})$	$\alpha°$	β	$\Omega_\delta(cm^{-1})$	$\gamma°(\Omega)$	$\gamma_\delta(\Omega)$
2600	66	0.7985	0.3275	30	0.125	0.275

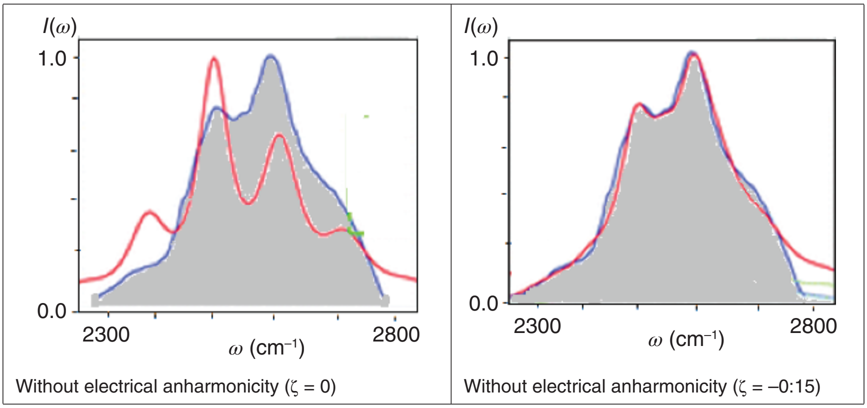

Without electrical anharmonicity (ζ = 0)

Without electrical anharmonicity (ζ = –0:15)

Figure 1.29 Gaseous $(CH_3)_2$ O· · ·HCl complex. Effect of the ζ electrical anharmonicity parameter. Source: Rekik et al. 2017 [17]/ Royal Society of Chemistry.

Table 1.23 Parameters used for fitting the lineshapes of gaseous $(CH3)_2O\cdots HCl$ complex.

	ω°(cm^{-1})	Ω(cm^{-1})	α°	$\gamma^\circ(\Omega)$	$\gamma(\Omega)$	ζ
$CH_3O^{\cdot\cdot}HCl$	2579	106	0.721	0.30	0.20	−0.15

They demonstrated the ability of a simple anharmonic model of the dipole moment function of the X–H stretching band to explain a set of spectroscopic features of hydrogen bonding formation.

1.4 Conclusion

In this chapter, before exposing the experimental tests of our theory of IR spectra of cyclic H-bonded dimers, we have given the main theoretical elements to allow its use, from the basic idea of an anharmonic coupling between a mode of low frequency and a mode of high frequency, through the introduction of various effects such as the Davydov effect, Fermi resonances or electrical anharmonicity.

The good results obtained for the adjustment of the experimental spectra by those who have systematically used this theory can find in this work a good recognition of their efforts towards a good understanding of the behavior of hydrogen bonds.

1.5 Acknowledgment

The authors are grateful to Ms. Joëlle Sulian for the preparation of several figures in this manuscript.

References

1 Blaise, P., Wójcik, M.J., and Henri-Rousseau, O. (2005). *J. Chem. Phys.* 122: 064306.
2 Maréchal, Y. and Witkowski, A. (1968). *J. Chem. Phys.* 48: 3637.
3 Boulil, B., Henri-Rousseau, O., and Blaise, P. (1988). *Chem. Phys.* 126: 263.
4 Rösch, N. and Ratner, M. (1974). *J. Chem. Phys.* 61: 3344.
5 Henri-Rousseau, O. and Blaise, P. (1998). The infrared spectral density of weak hydrogen bonds within the linear response theory. *Adv. Chem. Phys.*, vol. 103 (eds. I. Prigogine and S.A. Rice), 1–186. New York: Wiley.
6 Blaise, P., Déjardin, P.-M., and Henri-Rousseau, O. (2005). *Chem. Phys.* 313: 177.
7 Sakun, V. (1985). *Chem. Phys.* 99: 457.
8 Abramczyk, H. (1985). *Chem. Phys.* 94: 91.
9 Robertson, G. and Yarwood, J. (1978). *Chem. Phys.* 32: 267.
10 Bratos, S. and Hadzi, D. (1957). *J. Chem. Phys.* 27: 991.

11 Chamma, D. and Henri-Rousseau, O. (1999). *Chem. Phys.* 248: 91–104.

12 Witkowski, A. and Wojcik, M. (1973). *Chem. Phys.* 1: 9–16.

13 Davydov, A. (1962). *Theory of Molecular Excitons*. New York: McGraw Hill.

14 Rekik, N., Al-Agel, F.-A., and Flakus, H.-T. (2016). *Chem. Phys. Lett.* 647: 107–113.

15 Rekik, N. and Wójcik, M.J. (2010). *Chem. Phys.* 369: 71–81.

16 Rekik, N., Suleiman, J., Blaise, P. et al. (2017). *Phys. Chem. Chem. Phys.* 19: 5917–5931.

17 Rekik, N. and Alshammari, M.F. (2017). *Chem. Phys. Lett.* 678: 222–232.

18 Henri-Rousseau, O. and Blaise, P. (2008). *Adv. Chem. Phys.* 139 (5): 245–496.

19 Blaise, P., El-Amine Benmalti, M., and Henri-Rousseau, O. (2006). *J. Chem. Phys.* 124: 024514.

20 Haurie, M. and Novak, A. (1965). *J. Chim. Phys.* 62: 146.

21 Benmalti, M.E.-A., Blaise, P., Flakus, H.T., and Henri-Rousseau, O. (2006). *Chem. Phys.* 320: 267–274.

22 Bournay, J. and Maréchal, Y. (1971). *J. Chem. Phys.* 55: 1230.

23 Auvert, G. and Maréchal, Y. (1979). *Chem. Phys.* 40: 51; *ibid*, p. 61.

24 Flakus, H.T. and Miros, A. (1999). *J. Mol. Struct.* 484: 103.

25 Flakus, H.T. and Chelmecki, M. (2002). *Spectrochim. Acta, Part A* 58: 179.

26 Issaoui, N., Ghalla, H., and Oujia, B. (2013). *J. Appl. Spectrosc.* 80 (1): 14–24.

27 Ghalla, H., Rekik, N., Michta, A., Oujia, B., and Flakus, H.T. (2010). *Spectrochim. Acta, Part A* 75-1: 37–47.

28 Fathi, S., Blaise, P., Ceausu-Velcescu, A., and Nasr, S. (2017). *Chem. Phys.* 492: 12–22.

29 Ghalla, H., Issaoui, N., and Oujia, B. (2012). *Int. J. Quantum Chem.* 112: 1373–1383.

30 Flakus, H.T., Jabonska, M., and Kusz, J. (2009). *Vib. Spectrosc.* 49: 174.

31 Rekik, N., Flakus, H.T., Jarczyk-Jedryka, A. et al. (2015). *J. Phys. Chem. Solids* 77: 68–84.

32 Rekik, N., Ghalla, H., and Hanna, G. (2012). *J. Phys. Chem. A* 116: 4495–4509.

33 Rekik, N., Salman, S., Suleiman, J. et al. (2019). *Chem. Phys.* 519: 110–125.

34 Rekik, N., Flakus, H.T., Hachula, B. et al. (2020). *Spectrochim. Acta, Part A* 237: 118302.

35 Asfin, R.E., Denisov, G.S., and Tokhadze, K.G. (2002). *J. Mol. Struct.* 608: 161–168.

36 Rekik, N., Alsaif, N., Flakus, H.T. et al. (2020). *Spectrochim. Acta, Part A* 242: 118728.

37 Lassegues, J.C. and Huong, P.V. (1972). *Chem. Phys. Lett.* 17: 444–446.